



Democratic and Popular Republic of Algeria

Ministry of Higher Education and Scientific Research

Larbi Tebessi University

Faculty of Exact Sciences and Sciences of Nature and Life

Department of Matter Sciences

MASTER'S THESIS

Field: Matter Sciences

Discipline: Physics

Option: Condensed Matter Physics

Theme:

**Shell Model description of the ^{28}Si , with $N=Z$:
Energy spectrum**

Presented by:

Mecheri Romaiissa

Doubia Randa

Board of Examiners:

Chair:	BOUMALI Abdelmalek	<i>Professor</i>	Larbi Tebessi University
Supervisor:	BOUHELAL Mouna	<i>Professor</i>	Larbi Tebessi University
Examiner:	AOUNALLAH Houcine	<i>M. C. A</i>	Larbi Tebessi University

Date of defence: 23/6/2021

Note:

Mention:



Déclaration sur l'honneur de non-plagiat
 (à joindre obligatoirement au mémoire, remplie et signée)



Je soussigné(e) *Dania Randa*
 Nom, Prénom : *Dania Randa*
 Régulièrement inscrit(e) en Master au département : *Sciences de la matière*
 N° de carte d'étudiant : *15 15 340 21722 / 15 15 340 23799*
 Année universitaire : *2020/2021*
 Domaine : *Sciences de la matière*
 Filière : *Physique*
 Spécialité : *Physique de la matière condensée*
 Intitulé du mémoire : *Shell model description of He²⁺ with N=Z : Energy spectrum*

Atteste que mon mémoire est un travail original et que toutes les sources utilisées ont été indiquées dans leur totalité. Je certifie également que je n'ai ni recopié ni utilisé des idées ou des formulations tirées d'un ouvrage, article ou mémoire, en version imprimée ou électronique, sans mentionner précisément leur origine et que les citations intégrales sont signalées entre guillemets.

Sanctions en cas de plagiat prouvé :

L'étudiant sera convoqué devant le conseil de discipline, les sanctions prévues selon la gravité du plagiat sont :

- L'annulation du mémoire avec possibilité de le refaire sur un sujet différent ;
- L'exclusion d'une année du master ;
- L'exclusion définitive.

Fait à Tébessa, le : *11/07/2021*

Signature de l'étudiant(e) :

[Signature]
 12 جويلية 2021
 رئيس المجلس التأسيسي
 ويتضمن
 عنوان اداري بالقرع الذي جعل التوقيع
 رسميا

Randa *Mechechi*



Democratic and Popular Republic of Algeria

Ministry of Higher Education and Scientific Research

Larbi Tebessi University

Faculty of Exact Sciences and Sciences of Nature and Life

Department of Matter Sciences

MASTER'S THESIS

Field: Matter Sciences

Discipline: Physics

Option: Condensed Matter Physics

Theme:

**Shell Model description of the ^{28}Si , with $N=Z$:
Energy spectrum**

Presented by:

Mecheri Romaïssa

Doubia Randa

Board of Examiners:

Chair:	BOUMALI Abdelmalek	<i>Professor</i>	Larbi Tebessi University
Supervisor:	BOUHELAL Mouna	<i>Professor</i>	Larbi Tebessi University
Examiner:	AOUNALLAH Houcine	<i>M. C. A</i>	Larbi Tebessi University

Date of defence: 23/6/2021

Note:

Mention:



Thesis achieved at

Laboratoire de Physique Appliquée et Théorique LPAT



Abstract

Nuclear shell model has been implanted to describe the energy spectra and electromagnetic transitions of a selected region of nuclei, using an effective interaction compatible with the chosen valence space.

In the last years, the region of sd nuclei has been the interesting subject of many experimental and theoretical researches. The basic features of these nuclei are the co-existence of normal positive parity states and intruder negative parity states at low excitation energies.

The USD (USDA/USDB) interactions describe correctly the normal positive parity states. On the other hand, the PSDPF interaction describes well the normal positive- and intruder negative- parity states.

The main aim of this work is the calculation of the spectroscopic properties of ^{28}Si , specifically, levels that has an astrophysical interest and the calculation of the electromagnetic transitions of the first excited states.

The obtained results will be compared to experimental data and a detailed discussion will be presented.

Résumé

Le modèle en couches nucléaire a été implémenté pour décrire les spectres énergétiques et les transitions électromagnétiques d'une région sélectionnée de noyaux, en utilisant une interaction effective compatible avec l'espace de valence choisi.

Dans ces dernières années, les noyaux de la région de la couche sd sont devenus un sujet intéressant pour de nombreuses recherches expérimentales et théoriques. Les caractéristiques de base de ces noyaux sont la coexistence d'états normaux de parité positive et intrus de parité négative à basses énergies d'excitation.

Les interactions USD (USDA/USDB) décrivent correctement les états normaux de parité positive. D'autre part, l'interaction PSDPF décrit bien les normaux états de parité positive et intrus négative.

L'objectif principal de ce travail est le calcul des propriétés spectroscopiques du ^{28}Si , plus précisément, des niveaux présentant un intérêt astrophysique et le calcul des transitions électromagnétiques des premiers états excités.

Les résultats obtenus seront comparés aux données expérimentales et une discussion détaillée sera présentée.

ملخص

تم إعداد نموذج الطبقات النووية لوصف أطياف الطاقة والانتقالات الكهرومغناطيسية لمنطقة منتقاة من الانوية، باستخدام تفاعل فعال متوافق مع فضاء التكافؤ المختارة. خلال السنوات الاخيرة، اصبحت منطقة طبقة الانوية sd موضوعا مثيرا للاهتمام للبحوث التجريبية والنظرية. الخصائص الأساسية لهذه الانوية هي تواجد حالات الزوجية الموجبة و السالبة الدخيلة في طاقة الإثارة المنخفضة. التفاعلات USD (USDA / USDB) تصف بشكل صحيح حالات الزوجية الموجبة العادية. من ناحية أخرى ، يصف التفاعل PSDPF حالات الزوجية الموجبة العادية و السالبة الدخيلة.

الهدف الرئيسي من هذا العمل هو حساب الخصائص الطيفية لـ ^{28}Si وبشكل أدق المستويات الطاقوية التي لها جانب و دور هام في الفيزياء الفلكية وحساب الانتقالات الكهرومغناطيسية للحالات المثارة الأولى.

ستتم مقارنة النتائج المحصل عليها مع النتائج التجريبية المتوفرة وسيتم تقديم مناقشة مفصلة لها.

Dedication

"Success is not final; failure is not fatal: It is the courage to continue that counts."

First of all, Alhmdoulilah, I have successfully completed this work, I dedicate this humble work to my parents "RACHID" and "BRINO" you are the reason to be here.

To my soul mate brothers "REDHA" and "AYMEN" you are one-of-a-kind and I'm lucky to be your sibling.

To my dear sisters "AHLEM" and "AZIZA" You are my mirror, shining back at me with a world of possibilities. You are my witness, who sees me at my worst and best, and loves me anyway.

To my sister in law "HANENE" and my grand mother "Yamma" I love you so much. .

To my happiness, joy, honesty, innocent children "Lina" "Taline" "Djawed".

To all my family especially "Hmaidia" and to our friends and colleagues at the university thanx you so much.

To my dear, my partner and my intimate friend RANDA, in remembrance of our sincere and deep friendship and of the moments pleasant that we spent together and I'm so sorry for every time I lost my temper, I wish you a lifetime of joyous happiness.

I want say that the real test is not whether you avoid this failure, because you won't. It's whether you let it harden or shame you into inaction, or whether you learn from it; whether you choose to persevere.

MECHERI Roumaissa

First of all, thanks to Allah for the strength he gave me to stand here and achieve this work, then unusually I would thank myself for the durability and the steadfastness against hurdles and obstacles.

I would dedicate this humble work to the only person who stands always by my side and supports me, to my eternity heaven and infinite happiness, to my mother "LINDA", this is your success and prayers over nights.

To my father "KAMEL", keep your head up your daughter finally did it.

To the first love of my life, my safe haven, to my only brother "AYMEN"; you told me once that you will always be proud of me whatever it was, I would say that I'm proud of you more.

To my two little angels, with you both, I am strong enough to face everything and to stand where I am. To my sisters "RAOUIA" and my little baby love "MAY IKRAM".

To all my friends from elementary to university thanks all of you for the good moments we spend together, my best wishes for you.

To my partner, and dear friend "ROUMAÏSSA", thanks for the good moments you gave me, for our deep friendship, I apology for losing my temper many times, you mean too much to me, I wish you always the best luck and happiness.

Special thanks to my teacher BOUHELAL Mouna for believing, supporting and guiding me till the last moment in this work, thank you for your precious advices and instructions.

To every person has supported me in my journey.

DOUBIA Randa

Aknowledgements

To our supervisor,

Prof. BOUHELAL Mouna, we thank you for the kindness and spontaneity that you showed, for your support and understanding, and for your advices, we will always be grateful for your interest and the pretty moments you gave it to us.

We would like to acknowledge our committee members Prof. BOUMALI Abdelmalek for chairing our thesis and AOUNALLAH Houcine for examining our work. Thank you for joining our committee.

We would also like to acknowledge Prof. YOUSFI Mohammed and Prof. BOULDJEDRI Abdelhamid from university of Batna for giving us a helping hand when we asked for it, and for their valuable advices. Our endless thanks for you.

Table of contents

Abstract.....	III
Résumé.....	IV
ملخص.....	V
Dedication.....	VI
Acknowledgements.....	VII
Table of Contents.....	VIII
List of Tables.....	X
List of Figures.....	XI
List of Symbols.....	XII
General introduction.....	1
Chapter I: Silicon and nuclear astrophysics	4
I.1. Nuclear structure physics	5
I.2. Nuclear astrophysics	5
I.3. Nucleosynthesis	5
I.3.1. Big bang nucleosynthesis	6
I.3.2. Stellar nucleosynthesis ($A \leq 60$)	6
I.3.3. Supernova nucleosynthesis	6
I.4. Silicon burning process	7
I.5. General characteristic of silicon.....	7
I.6. Application of Silicon.....	8
Chapter II: Spectroscopic study of sd-shell nuclei using the shell model framework.....	11
II-1. Nuclear models.....	11
II.1.1. Liquid drop model.....	11
II.1.2. Magic numbers.....	12
II.1.3. Shell model.....	14
II.1.3.1. Independent particle model.....	14
The harmonic oscillator potential.....	14

The spin-orbit interaction.....	15
II.1.3.2. General N-body problem in the nucleus.....	16
II.1.3.3. Ingredients of the shell model.....	17
Choice of the valence space.....	17
Effective interaction.....	18
Shell model codes.....	18
II.2. Sd shell nuclei.....	18
II.2.1. Sd-shell nuclei states.....	19
II.2.1.1. Normal states.....	19
II.2.1.2. Intruder states.....	19
Positive parity intruder states.....	19
Negative parity intruder states.....	19
II.3. PSDPF interaction.....	20
II.3.1. Shell model ingredients in case of sd-shell nuclei.....	20
II.3.2. Positive and negative parity states description.....	20
II.3.3. Isospin.....	22
II.4. Electromagnetic transitions.....	22
II.4.1. Selection rules.....	22
II.4.2. Operators.....	24
II.4.2.1. Electric operator.....	24
II.4.2.2. Magnetic operator.....	24
II.4.3. Electromagnetic transitions probabilities.....	24
II.5.4. Electromagnetic transitions in sd nuclei.....	25
chapter III: Shell model description of ^{28}Si energy spectrum	28
III.1. Experimental review of the energy spectrum of ^{28}Si	28
III-2. Results and discussion.....	31
III.2.1. Energy spectrum.....	31
III-2.2. Electromagnetic transitions.....	37
Conclusion.....	40
Bibliography.....	42

List of Tables

Table N°	Title	Page
Table II-1	End Products issued from natural radioactive series [20].	13
Table II-2	Gamma transition multipolarity.	23
Table II-3	Weisskopf single-particle widths Γ_W (W. u.) in MeV [25].	25
Table II-4	Adjusted parameters for the transitions E2, M1 and E3.	25
Table III-1	J^π assignment states in 2015 [43].	29
Table III-2	Updated J^π assignments obtained in 2020 [44].	29
Table III-3	The energy spectrum of the ^{28}Si .	32
Table III-4	High spin states.	37
Table III-5	Comparison experimental [41] versus calculated spectroscopic properties of the ^{28}Si .	37

List of figures

Figure N°	Title	Page
Figure I-1	Components of the universe [2].	4
Figure I-2	Chart resumes nucleosynthesis.	5
Figure I-3	Image of a supernova remnant known as N132D in the Large Magellanic Cloud [1]	7
Figure I-4	Characteristic of silicon 28 element [11]	8
Figure II-1	Binding energy of last neutron (MeV) per neutron number N [20].	12
Figure II-2	Sharp of absorption cross-sections σ (mb) per neutron number N [20].	13
Figure II-3	Natural abundance of lead isotopes [21].	13
Figure II-4	Split of the degenerated states with n, l into states with n, l and j	16
Figure II-5	Diagram of the single-particle orbitals within the shell model [25].	17
Figure II-6	Valence space diagram.	18
Figure II-7	Chart of sd shell nuclei [19].	19
Figure II-8	sd nuclei with known negative parity intruder states [19].	20
Figure II-9	Configurations of the first excited states 2^+ and 3^- in $^{28}_{14}\text{Si}$.	21
Figure II-10	Gamma emission and absorption of a nucleus.	23
Figure III.1	Schematic diagram of the proton rich process in ^{27}Al and the decay of ^{28}Si [46].	31

List of symboles

PAMELA	Payload for Antimatter Matter Exploration and Light-nuclei Astrophysics
SiPM	Silicon Photomultiplier
A	Atomic number
Z	Number of protons
LIDAR	Light Intensity Detection and Ranging
N	Number of neutrons
$V_{O,H}$	Harmonic-Oscillator potential
H_0	The Hamiltonian of independent movement of nucleons in the nucleus
ω	The harmonic-Oscillator frequency
h_i	The Hamiltonian of an individual nucleon
V_{ij}	Two-body interaction between the nucleons i and j
H_r	The residual interaction
USD	sd-shell universal interaction compatible with sd valence space
USDA	sd-shell universal interaction compatible with sd valence space (updated version of the USD interaction)
USDB	sd-shell universal interaction compatible with sd valence space (updated version of the USD interaction)
PDSPF	Effective interaction for sd-shell nuclei compatible with p-sd-pf valence space
$0\hbar\omega$	(0 particle-0 hole jump) denotes the positive parity states
$1\hbar\omega$	(1 particle-1 hole jump) denotes the negative parity states
E_i	Initial state energy
E_f	Final state energy
μ_N	The nuclear magneton
Γ_γ	The transition widths
Γ_W	Weisskopf estimation
τ_m	The average life
$T_{1/2}$	Half-life
EL	Electrical transition

ML	Magnetic transition
e_p	The free charge of proton
e_n	The free charge of a neutron
π_γ	The parity of a transition (of γ photon)
ΔE	The difference between calculated and experimental energy
g^l, g^s	Gyromagnetic factors of orbit and spin
$e(k)$	The nucleon k effective charge
r-process	Rapid neutron-capture process
s-process	Slow neutron-capture process
p-process	Proton capture process
α – process	Alpha particle process

General introduction

Nuclear astrophysics is a collaboration of nuclear physics and astrophysics that aims to understand how nuclear process shape the cosmos, including the chain of fusion events or the nucleosynthesis. Another purpose of nuclear astrophysics is the connection between the properties of atomic nuclei and those of planets, stars, and galaxies.

Astrophysics is a field of space science that applies the laws of physics and chemistry to explain the birth, life and death of stars, planets and galaxies.

Nucleosynthesis is the creation of new atomic nuclei by nuclear reactions in massive stars over the fusion of lighter elements into heavier ones.

Silicon is one of the main light elements that were formed in the early epochs, only a few seconds or minutes after the Big Bang. This formation gave it an importance among the other elements and a widespread in solar system and earth crust; hence, it is more useful in the technological field as well as the medical one.

Nuclear models were developed to describe how the protons and neutrons are arranged within the nucleus. The most successful nuclear model is the shell model. The main assumptions of this strong nuclear tool is that nucleons are moving in an independent way in an average field; it is composed of a central potential and the most used is the harmonic oscillator potential. The spin-orbit interaction was indispensable in this case to describe magic numbers; however, the description of any nuclei needs a compatible interaction with the chosen valence space.

The sd shell nuclei, having number of protons Z and neutrons N between 8 and 20. This region of nuclei is located between the doubly magic nuclei ^{16}O and ^{40}Ca . At low excitation energy, the experimental spectra of these nuclei are characterized by the coexistence of normal positive parity states and intruder negative parity states.

The normal states with positive parity have been already well described by the shell model using the USD (USDA/USDB) interactions within the valence space with an ^{16}O inert core. However, the PSDPF interaction developed by M. BOUHELAL describes, in addition of the normal states, the intruder negative parity states where the model space is composed of the three major shells p-sd-pf and a ^4He as an inert core.

The primary objective of our thesis is the calculation, using PSDPF, of the spectroscopic properties of the ^{28}Si , particularly, levels of astrophysical interest. This nucleus, with $N=Z$, is situated in the middle of the silicon isotopic chain that is situated in the middle of sd shell nuclei

nuclei area. The ambiguous states have been determined based on the comparison experimental versus theory.

The outline of this manuscript contains three main chapters:

- **Chapter I:** Presents an introduction to Silicon interest in nuclear astrophysics, focusing on universe evolution.
- **Chapter II:** Presents a brief overview about nuclear shell model, the sd-shell nuclei, and the PSDPF interaction.
- **Chapter III:** Expose a discussion of the spectroscopic properties results and their comparison to experimental data mainly those concerning states of astrophysical interest of ^{28}Si .

Our dissertation will end by a general conclusion.



Chapter I

Chapter I

Silicon and nuclear astrophysics

Our universe is believed to have formed about 15 billion years ago in a dense, hot ball of fire, the big bang. Over time, the universe has expanded and cooled. After a microsecond, a soup of quarks and gluons condensed into protons and neutrons and the era of nuclear physics began. After another 10 seconds, the universe had cooled to the point where the lightest nuclei, the isotopes of hydrogen, helium and a tiny amount of lithium, could form. These nuclei are the ashes of the first elemental formation processes - everything that follows begins with nuclear reactions between the nuclei of these three elements. [1]. **Figure I-1** presents the formation of the universe.

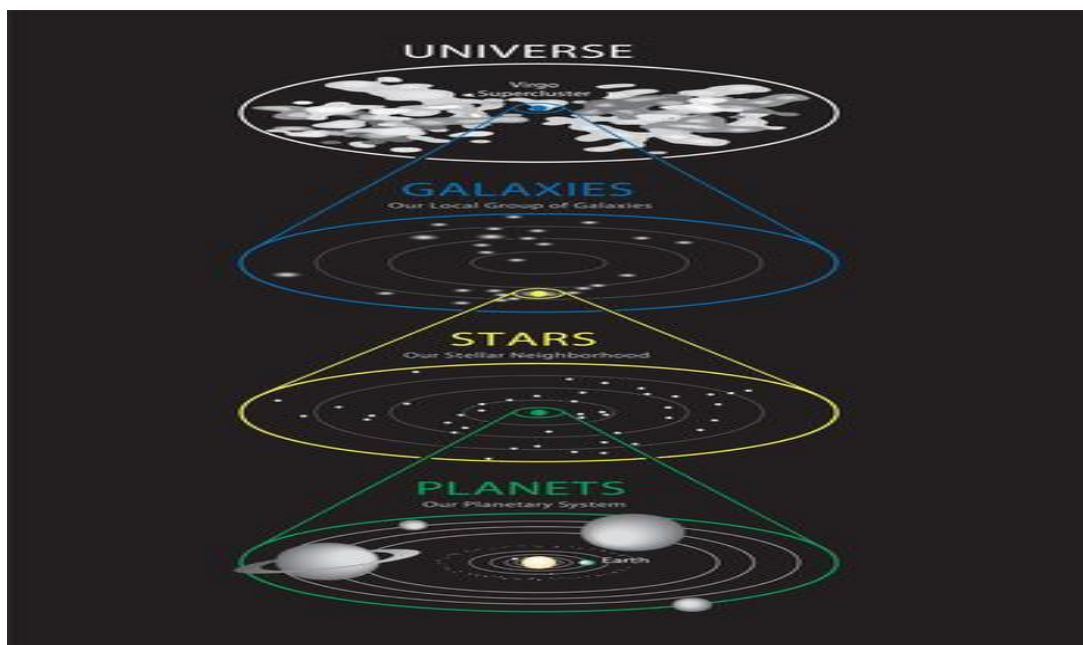


Figure I-1: Components of the universe [2].

Silicon is the seventh most abundant element in the universe, and it is very common on Earth. In the Earth's crust, silicon is the second most abundant element [3]. Pure silicon is produced by heating silicon dioxide with carbon at temperatures approaching 2200°C. Silicon can get quite pure, and even different isotopes can get pure. Special techniques are able to make silicon that is 99.9999% pure ^{28}Si . Silicon is used extensively in electronics because of its semiconducting properties [3].

I.1. Nuclear structure physics

Nuclear structure physics pursues to understand the nature of nucleonic matter (its phases and modes at different distance scales). It tries to develop a unified microscopic description of the nucleus focusing on the various and rare phenomena of the nucleus by probing the characteristic single-particle and collective excitation modes [4].

I.2. Nuclear astrophysics

Nuclear astrophysics is interested in the influence and impact of microscopic nuclear structure and nuclear reaction physics on the development and evolution of stars macroscopic systems in our Universe [4].

I.3. Nucleosynthesis

Nucleosynthesis refers to the production of elements that compose the baryonic matter of the universe. We now understand that nuclear processes, operating by nuclear processes, both in the early universe and in stars, are responsible for the synthesis of the elements. This universal nuclear history of the matter is written in the compositions of its various components: stars, interstellar (and intergalactic) gas and dust, meteorites, and cosmic rays [1].

There are three major types of nucleosynthesis summarized in the following subsections, which are shown on Figure I-2.

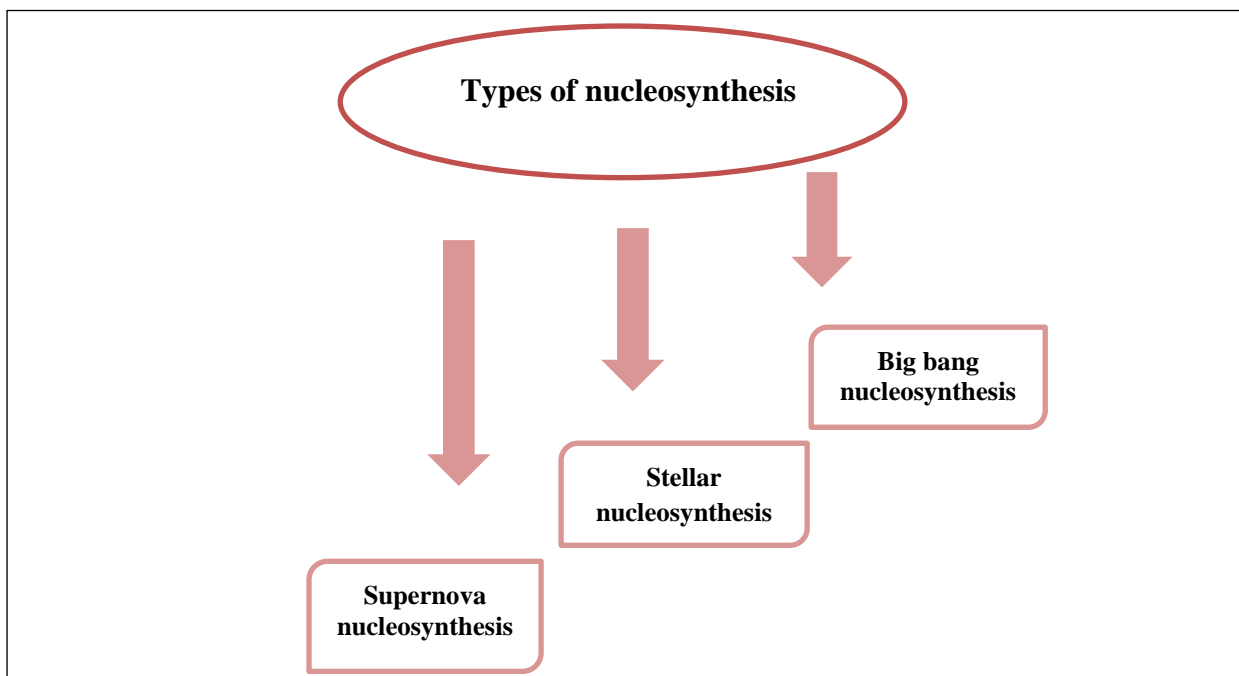


Figure I-2: Chart resumes nucleosynthesis.

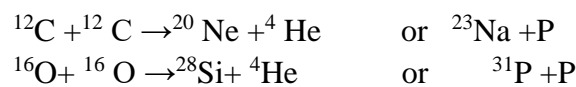
I.3.1. Big bang nucleosynthesis

The big bang created the light nuclei ^1H , ^2H , ^3He , ^4He , and ^7Li . Reactions between nuclei in the interstellar gas and high-energy cosmic rays also form these elements, as may interactions of neutrinos with heavier nuclei in supernovae [1].

I.3.2. Stellar nucleosynthesis ($A \leq 60$)

Combining the protons and neutrons together from the nuclei of lighter elements creates elements in stars; this process is called stellar nucleosynthesis. All of the atoms in the universe began as hydrogen. Fusion inside stars transforms hydrogen into helium, heat, and radiation. Heavier elements are created in different types of stars as they die or explode [5].

When the helium fuel begins to be exhausted, gravitational collapse sets in again. The star then heats up enough to ignite ^{12}C and ^{16}O burning, which permits such reactions as [6].

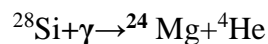


At temperatures on the order of 10^9 K, where the Coulomb barrier can be more easily penetrated. In addition to these reactions, other α particle and nucleon capture reactions can also occur. For example; ^{14}N may be present in second-generation stars, originally formed from ^{12}C as part of the carbon cycle of proton-proton fusion discussed in Section 14.3. Alpha capture reactions can produce the chain $^{14}\text{N} \rightarrow ^{18}\text{O} \rightarrow ^{22}\text{Ne} \rightarrow ^{26}\text{Mg} \dots$ Reactions other than (α, γ) , including (α, n) or (p, γ) will occur, with somewhat less probability [6].

The last step in the production of near-mass 60 nuclei is the combustion of silicon, which is actually a complex sequence of reactions that take place quickly. But in conditions close to equilibrium deep within the warm stellar interiors. The Coulomb barrier is too high to allow direct formation by reactions such as [6].



Instead, what happens are combinations of photo-dissociation reactions (γ, α) , (γ, p) or (γ, n) followed by the capture of the dissociated nucleons and many other similar reactions [6].



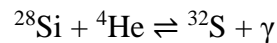
I.1.3.1. Supernova nucleosynthesis

Supernova nucleosynthesis is the nucleosynthesis of chemical elements in supernova explosions. In sufficiently massive stars, nucleosynthesis by fusion of lighter elements into heavier elements occurs during sequential hydrostatic combustion processes called the combustion of helium, carbon, oxygen and silicon, in which the ash of a nuclear fuel becomes, after heating by compression, the fuel for the next combustion step [7].

After a star completes the process of burning oxygen, its core is mostly composed of silicon and sulfur. If it has a sufficiently high mass, it contracts further until its core reaches

temperatures between 2.7 and 3.5 billion Kelvin (230-300 KeV). At these temperatures, silicon and other isotopes undergo photo-ejection of nucleons by energetic thermal photons (γ) ejecting in particular alpha particles (^4He) [8].

The nuclear combustion process of silicon differs from the earlier fusion stages of nucleosynthesis in that it involves a balance between the capture of alpha particles and their reverse photo-ejection which establishes the abundance of all alpha particles elements in the following sequence in which each alpha particle capture shown is opposed by its reverse reaction, namely, photo-ejection of an alpha particle by abundant thermal photons [8].



The Hubble Space Telescope image of a supernova remnant known as N132D in the Large Magellanic Cloud. Massive stars synthesize elements in their nuclei by nuclear fusion and is presented in Figure I-3.

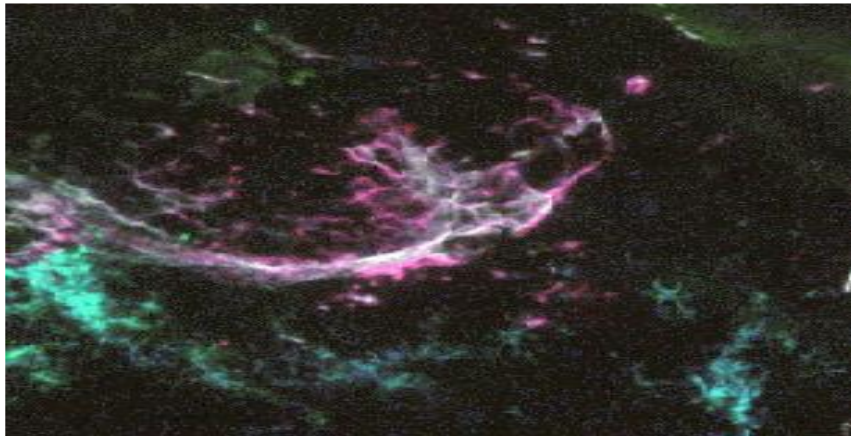


Figure I-3: Image of a supernova remnant known as N132D in the Large Magellanic Cloud [1].

I.4. Silicon burning process

In astrophysics, the combustion of silicon is a very brief sequence of nuclear fusion reactions that occur in massive stars. The combustion of silicon is the last step in the fusion of massive stars that no longer have the fuels that fuel them during their long lives in the main sequence of the Hertzsprung-Russell diagram. It follows the previous stages of the combustion processes of hydrogen, helium, carbon, neon and oxygen [9].

The combustion of silicon begins when gravitational contraction raises the star's core temperature to 2.7 to 3.5 billion Kelvin (GK). The exact the temperature depends on the mass. When a star has completed the combustion phase of silicon, no further fusion is possible. The star catastrophically collapses and may explode in what is called a Type II supernova [9].

I.5. General characteristic of silicon

- 7th most abundant element in the universe and the 2nd on earth [3].
- **Most common isotopes:** ^{28}Si (92% natural abundance) [3].
- **Density:** 2.3296 grams per cubic centimeters [3].

- **Melting point:** 1687 K (1414 C) [3].
 - **Most common isotopes:** ^{28}Si (92% natural abundance) [3].
 - **Boiling point:** 3538 K (3265 C) [3].
 - **Group number:** 14 [3].
 - **Chemical symbol:** Si.
 - **Molecular weight:** 28.09.
 - **Appearance (form):** Solid.
 - **Color:** Silvery metallic.
 - **Odor:** Odorless.
 - **Atomic number:** 14.
- **Description of first aids measures:**
1. **In case of skin contact:** Get medical aid. Flush skin with plenty of water for at least 15 minutes while removing contaminated clothing and shoes. Wash clothing before reuse [10].
 2. **In case of eye contact:** Flush eyes with plenty of water for at least 15 minutes. Occasionally lifting the upper and lower eyelids. Obtain medical attention [10].

Figure I-4 summarizes the deferent characteristic of the Silicon element.

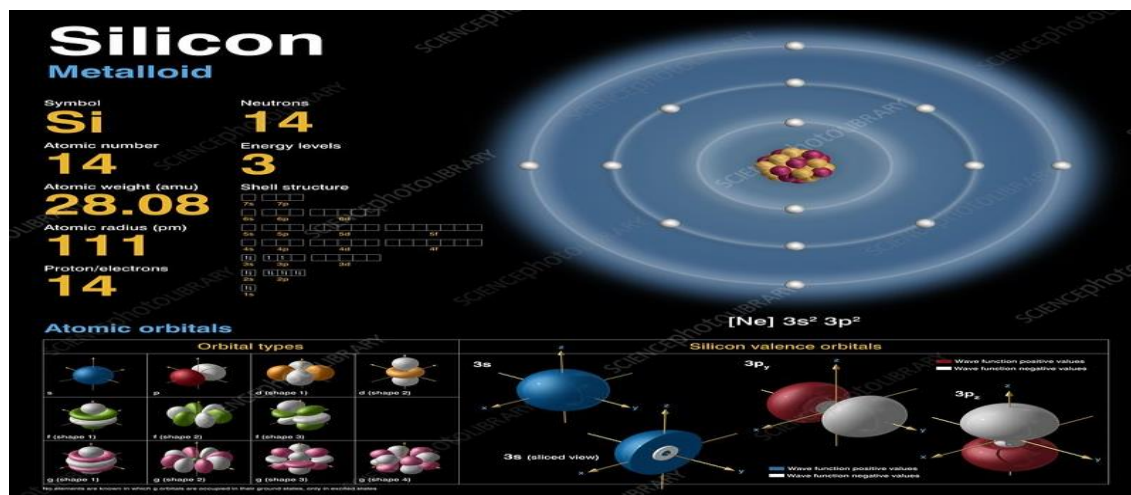


Figure I-4: Characteristic of the Silicon 28 element [11].

I.6. Applications of silicon

- The PAMELA experiment (a Payload for Antimatter Matter Exploration and Light-nuclei Astrophysics) is a satellite device designed to study charged particles in cosmic radiation with particular emphasis on antiparticles (a silicon-tungsten electromagnetic

calorimeter), which allows antiparticles to be reliably identified from a large background of other charged particles [12].

- The PAMELA mission is devoted to the study of dark matter, baryonic asymmetry in the Universe, the generation and propagation of cosmic rays in our galaxy and the solar system, and studies on solar modulation and the interaction of cosmic rays with the earth's magnetosphere [12].
- Silicon Photomultiplier: The silicon photomultiplier (SiPM) is an established device of choice for a variety of applications; for example. distance measurements in LIDAR, astrophysics, quantum cryptography and related applications as well as in high energy physics [13].
- SiPMs show extremely good single photon detection capability and excellent timing properties rendering them promising candidates for single photon counting applications [13].
- The element silicon is used extensively as a semiconductor in solid-state devices in the computer and microelectronics industries. For this, hyper pure silicon is needed. The silicon is selectively doped with tiny amounts of boron, gallium, phosphorus or arsenic to control its electrical properties [14].
- Silicon carbides are important abrasives and are also used in lasers [14].
- Granite and most other rocks are complex silicates, and these are used for civil engineering projects. Sand (silicon dioxide or silica) and clay (aluminum silicate) are used to make concrete and cement. Sand is also the principal ingredient of glass, which has thousands of uses. Silicon, as silicate, is present in pottery, enamels and high-temperature ceramics[14].

In this chapter, we presented a brief introduction nuclear astrophysics accentuating on the importance of Silicon in astrophysics, which is the area of our interest.

One of the isotopes that has an astrophysical interest is ^{28}Si , which will be studied in the art of shell model. This model will be described in the next chapter.



Chapter II

Chapter II

Spectroscopic study of sd-shell nuclei using the shell model framework

Neutrons and protons are known to be the nuclear constituents; the nucleons, the absence of a fundamental understanding of the nuclear force governing these nucleons made it difficult to determine the structure of the nucleus. It is not surprising therefore, that, instead of a theory, phenomenological models of the nucleus were constructed to accommodate the many remarkable experimental findings [15].

Nevertheless, each model has a flaw; but overall; these models describes well the nuclear features as well as the stability and collectivity behaviors.

In this chapter, we will present a brief overview about the most known nuclear models, a definition of the sd shell nuclei zone and the PSDPF interaction. This chapter will end by a short review about the electromagnetic transitions.

II.1 Nuclear models

II.1.1 Liquid drop model

The liquid drop model of the nucleus, formulated by George Gamow in 1929, and developed by Niels Bohr and John Wheeler. In 1938, Austrian physicists Lise Meitner and Otto Frisch used this model to explain nuclear fission [16].

A drop of incompressible liquid and the nucleus are similar or more accurately identical. The high-energy scattering experiments showed that the interior of all nuclei is identical to the charge density and the nucleon density. The big and small nuclei are like the big and small drops of a liquid, the surface effects of nuclei are shown in analogy with the surface of the liquids surface tension. The shape of all nuclei is nearly spherical like the drops of a liquid. The explanations for fission and fusion are encoded in this model. Two small liquid drops combine to make a big drop and a big liquid drop breaks into small drops [16]. In this model, the individual quantum properties of nucleons are completely ignored [16]. In this case, we can assume that nucleus is composed of a stable central core of nucleons where the nuclear force is completely saturated [16].

After a series of functions, equations and assumptions, the binding energy per nucleon of nuclei with mass number A ; using the semi-empirical formula of Weizsäcker given by [16]:

$$B(A, Z) = a_v A - a_s A^{2/3} - a_c \frac{Z(Z-1)}{A^{1/3}} - a_a \frac{(A-2Z)^2}{A} \pm \delta A^{-1/2} \quad (1)$$

Where all the coefficients a_v, a_s, a_c, a_a and δ are assumed to be positive. The fourth term implies that, unless $N = Z$, the binding energy will contain a positive contribution that will destabilize the nucleus [16].

In the last term, the positive sign for δ is chosen for odd-odd nuclei, implying that such nuclei are relatively unstable; for even-even nuclei, the sign of δ is taken as negative, implying greater stability. For odd- A nuclei, the value of δ is chosen to be zero [16].

The following values, obtained empirically, refers to Weizsäcker coefficients [16]:

$$a_v \approx 15.67 \text{ MeV}$$

- $a_s \approx 17.23 \text{ MeV}$

- $a_c \approx 0.714 \text{ MeV}$

- $a_a \approx 93.15 \text{ MeV}$

- $\delta = \begin{cases} -\delta_0 & \text{for even - even nuclei} \\ 0 & \text{for odd - even nuclei} \\ +\delta_0 & \text{for odd - odd nuclei} \end{cases}, \text{Where } \delta_0 = 11.2 \text{ MeV.}$

By the time, the empirical evidences showed that nuclides with Z or N equals to 2, 8, 20, 28, 50, 82 and 126 are comparatively more stable. These numbers called magic numbers. The liquid drop model could not explain the extra stability associated with magic numbers [15].

II.1.2. Magic numbers

Discovered by Maria Goeppert-Mayer [17] and Otto Haxel, J. Hans D. Jensen and Hans Suess [18], nuclei with Proton number Z or neutron number N equal to 2, 8, 20, 28, 50, 52, 126 are more stable than the nearby nuclei. Magic nuclei are nuclei with magic Z or N . Further, the doubly magic nuclei are with magic N and Z [18].

Special features of magic nuclei

1. The shape of the neutron (proton) separation energies (the energy required to remove the last neutron (proton)) has peaks if N or Z is equal to a magic number [20]. Figure II-1 presents a chart that explains the binding energy of last neutron per neutron number N that illustrates well these peaks [21].

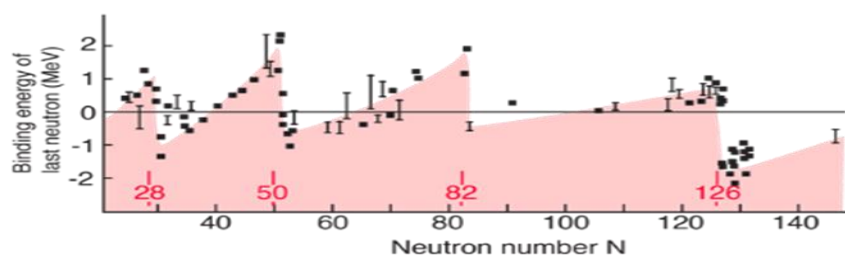


Figure II-1: Binding energy of last neutron (MeV) per neutron number N [20].

2. If N is a magic number then the cross-section for neutron absorption is much lower than for other nuclides [20]. See figure II-2.

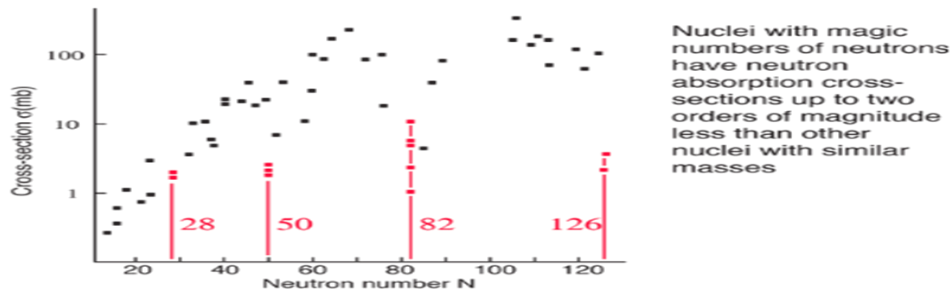


Figure II-2: Sharp of absorption cross-sections σ (mb) per neutron number N [20].

3. Elements with Z equal to magic number have a larger natural abundance than those of nearby elements [20], Figure II-3 explains more this feature.

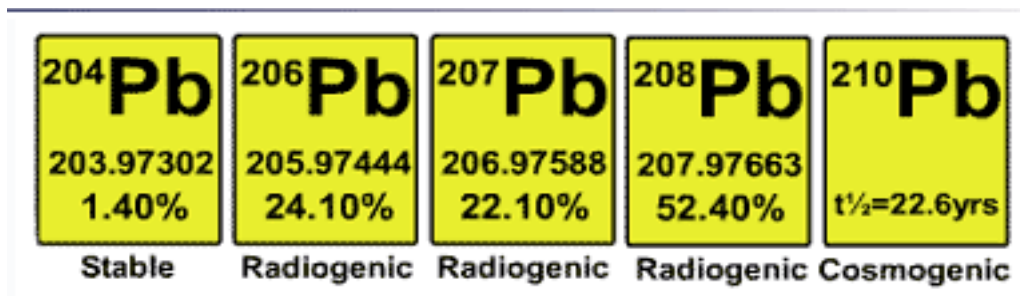


Figure II-3: Natural abundance of lead isotopes [21]

4. Stable elements at the end of a natural radioactive series have a magic number of proton and neutron [20].

According to table II-1, the end product have 82 protons and the Bismuth has 126 neutrons and those are magic numbers. The lead 208 is a doubly magic with $Z=82$; $N=126$.

Series	First decay	End product
Thorium	$^{232}\text{Th} \rightarrow ^{228}\text{Ra} + \alpha$	^{208}Pb
Neptunium	$^{237}\text{Np} \rightarrow ^{233}\text{Pa} + \alpha$	^{209}Bi
Uranium	$^{238}\text{U} \rightarrow ^{234}\text{Th} + \alpha$	^{206}Pb
Actinium	$^{235}\text{U} \rightarrow ^{231}\text{Th} + \alpha$	^{207}Pb

Table II-1: End Products issued from natural radioactive series [20].

II.1.3. Shell model

The shell model is one of nuclear structure models using the individual quantum properties of a problem of N-body.

As a first approximation, the basic assumption in the nuclear shell model is that each nucleon (proton or neutron) is moving in an independent way within an average field created by the (A-1) nucleons [22].

II.1.3.1. Independent particle model

The independent-particle model suppose that the nucleons are attracted in the center of the nucleus under the effect of a net potential-well produced by the nuclear force that acts between nucleons. The most used potential is the harmonic oscillator potential [23].

➤ The harmonic oscillator potential

A Hamiltonian and a choice of coordinate basis, spherical or Cartesian, define the harmonic oscillator basis [24].

It is assumed that the interaction between one nucleon and the (A-1) nucleon can be approximated by a central potential, the simplest one is the harmonic oscillator potential, which can be written as [25]:

$$V(r) = \frac{1}{2} m \omega^2 r^2 \quad (2)$$

With: ω is the frequency of the harmonic oscillation potential, r presents the distance between nucleon and the origin and m is the nucleon mass.

The nuclear Schrödinger equation in the harmonic oscillator takes the form:

$$H_0 \phi = E_0 \phi \quad (3)$$

With:
$$H_0 = T + V = \frac{p^2}{2m} + \frac{1}{2} m \omega^2 r^2 \quad (4)$$

$$H_0 = \sum_{i=1}^A (t_i + V_i) = \sum_{i=1}^A \left(\frac{p_i^2}{2m} + \frac{1}{2} \omega^2 r_i^2 \right) \quad (5)$$

Where the Hamiltonian of the independent particles is

$$H_0 = \sum_{i=1}^A h_i \quad (6)$$

$$h_i = t_i + \frac{1}{2} m \omega^2 r^2 = \frac{p_i^2}{2m} + \frac{1}{2} m \omega^2 r^2 \quad (7)$$

Eigen functions can be given as:

$$\Phi_{n_l m_l}(r) = R_{n_l}(r) Y_l^{m_l}(\theta, \varphi) \quad (8)$$

Here l and m_l are the quantum numbers of angular momentum and its projection, respectively. n is the radial quantum number.

The corresponding eigenvalues of the equation are given by [25]:

$$E_{n_l} = (N + 3/2)\hbar\omega ; \quad \hbar\omega = 41A^{-\frac{1}{3}} \text{ MeV} \quad (9)$$

N is the major oscillator quantum number $N = 2(n - 1) + l$ and determinate the harmonic oscillator major shells.

Unfortunately, the application of this potential allowed us to obtain only the first three magic numbers: 2,8,20.

As the harmonic oscillator potential failed to reproduce all the magic numbers, a new corrective term called the “edge-board effect” DL^2 ($D < 0$) has been added to the main Hamiltonian:

$$h_i = T_i + \frac{1}{2}m\omega^2 r^2 + DL_i^2 \quad (10)$$

With:
$$E_{n_l j}^i = \left(N + \frac{3}{2}\right)\hbar\omega + Dl(l+1)\hbar^2 \quad (11)$$

However, even after the addition of this new term, we still get only the first three magic numbers 2,8,20, but the degeneration on l is removed.

➤ The spin-orbit interaction

It was clear in 1940s that a central potential could not reproduce all the magic numbers. In 1949, Maria Goeppert Mayer and Hans Jensen suggested that inside the nucleus there is a strong spin-orbit interaction beside the central potential (Harmonic oscillator potential) [15]. This term is given by [25]:

$$V_{s,o} = f(r)\vec{l}_i \cdot \vec{s}_i \quad (12)$$

Now, the total single-particle Hamiltonian takes the following form:

$$h_i = T_i + \frac{1}{2}m\omega^2 r_i^2 + Dl_i^2 + f(r)\vec{l}_i \vec{s}_i \quad (13)$$

The Eigen function can be written as next:

$$\Phi_{n_l j m}(r, \sigma) = R_{n_l}(r) \sum_{m_l, m_s} \langle l m_l \frac{1}{2} m_s | j m \rangle |Y_l^{m_l}(\theta, \varphi) \rangle \quad m = m_l + m_s \quad (14)$$

The single particle energies or the eigenvalues are given by:

$$E_{n_l j} = (N + 3/2)\hbar\omega + Dl(l+1)\hbar^2 + \frac{\hbar^2}{2} \langle f(r) \rangle_{n_l} \begin{cases} -(l+1) & j = l - 1/2 \\ l & j = l + 1/2 \end{cases} \quad (15)$$

This shows that the originally degenerate single-particle states $j = l \pm 1/2$ are split up. The radial function $\langle f(r) \rangle_{nl}$ is negative and approximately given by [25]:

$$\langle f(r) \rangle_{nl} \approx -20A^{-\frac{2}{3}} \text{MeV} \quad (16)$$

The negative value reflects the experimental fact that the $j = l + 1/2$ energy states are lowered than the $j = l - 1/2$ energy states, it is clearly shown in figure II-4:

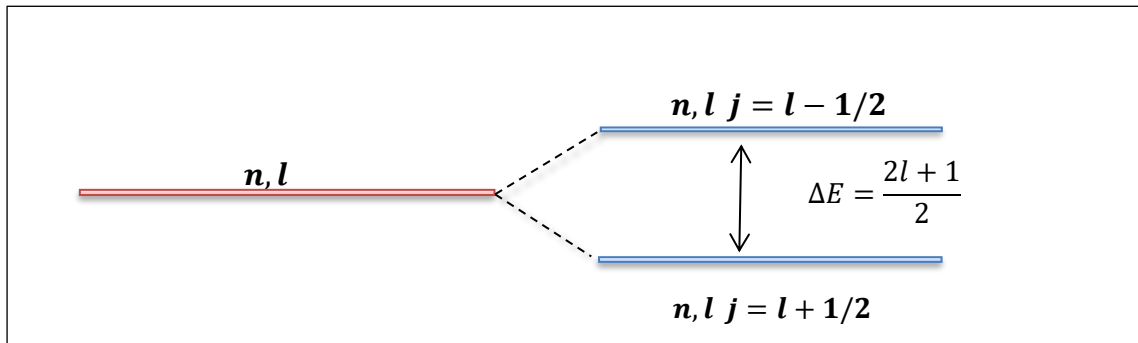


Figure II-4: Split of the degenerated states with n, l into states with n, l and j .

The spin-orbit interaction succeed, and leads to all the magic numbers 2, 8, 20, 28, 50, 82 and 126; the next figure (II-5) represent the single-particle orbitals.

II.1.3.2. General N-body problem in the nucleus

We mentioned previously that the basic assumption of the independent particle model is that nucleons are positioned in the center of the nucleus and moves in an independent way from each other in an average field with a mean-free path. However, this model is applicable only for the closed shells. Nucleons in the nucleus are interacting in pairs with a two-body forces V_{ij} and provide a zero-order overview of the structure of this nucleus. The Hamiltonian of this nucleus has the form [25]:

$$H = \sum_{i=1}^A (T_i + U_i) + (\sum_{i<j}^A V_{ij} - \sum_{i=1}^A U_i) = H_0 + H_r = \sum_{i=1}^A h_i + H_r \quad (17)$$

H_0 denotes the independent movement of nucleons in a one-body potential, h_i presents the individual Hamiltonian of a nucleon. H_r is the residual two-body interaction considered as a perturbation of the main H_0 Hamiltonian by an adequate choice.

The selection of the residual interaction is generally done by two methods: the shell model and the Hartee-Fock method.

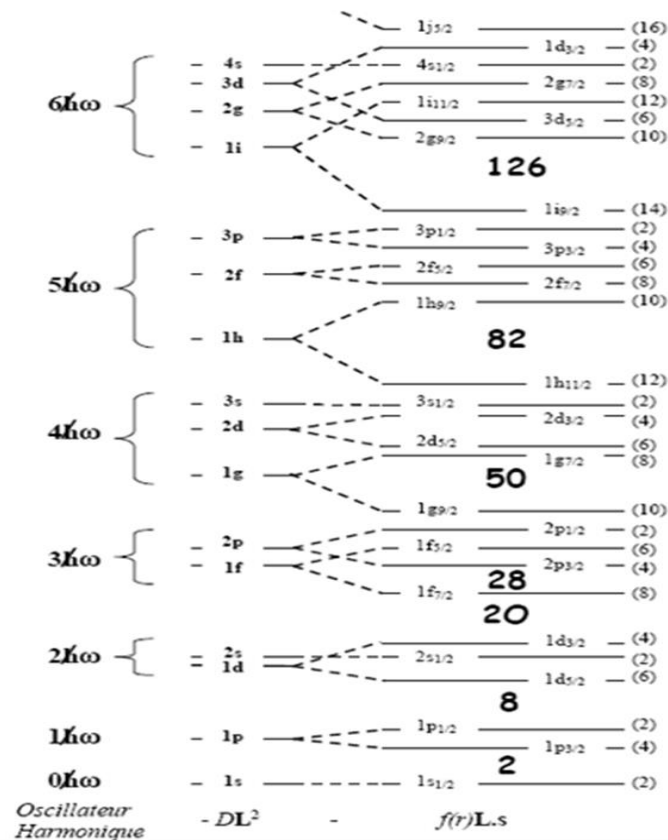


Figure II-5: Diagram of the single-particle orbitals within the shell model [25].

II.1.3.3. Ingredients of the shell model

The shell model calculation needs the functionality of the three next ingredients [19]:

1. Definition of valence space (inert core, active shells)
2. Derivation of a compatible effective interaction with the valence space.
3. Calculation code to build and diagonalize the Hamiltonians.

➤ Choice of the valence space

Schrodinger equation, in practice, is realized in an infinite dimension space. In the shell model approach, the Hilbert space is divided into three parts [19]:

- ✚ The inert core: contains all the full orbits. The core consists of N_c neutrons and Z_c protons.
- ✚ The valence space: corresponding to the set of orbits accessible to the valence nucleons. These orbits will be partially occupied by the valence nucleons ($Z_v=Z-Z_c$; $n_v=N-N_c$). See figure II-6.
- ✚ The external space: corresponding, by definition, to the empty orbits.

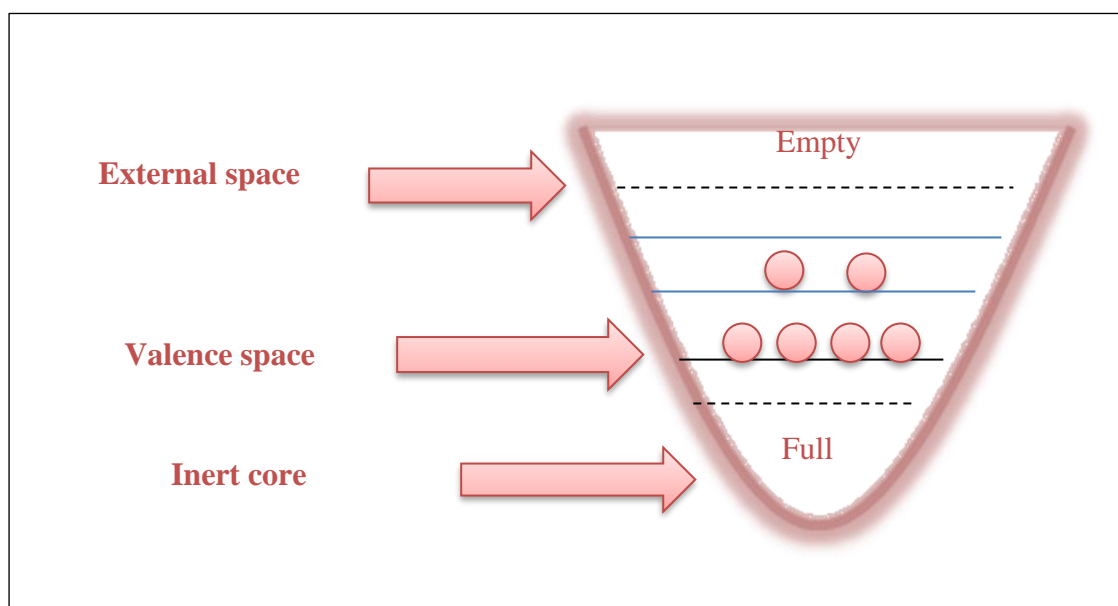


Figure II-6 : Valence space diagram.

➤ Effective interaction

Practically, each shell model calculation uses the residual and effective interaction between nucleons, because the nucleon-nucleon interaction cannot be used directly [19]. We have two types of effective interactions. The first one is the realistic effective interaction that is deduced directly from the nucleon-nucleon potentials (nucleon-nucleon scattering). The second one is the effective phenomenological interaction, based on the choice of a part of Hilbert space (truncated space, i.e. model space) and considering the individual energies and the two-body matrix elements as parameters to be adjusted to experimental data [26].

➤ Shell model codes

The two shell model codes developed in Strasbourg are ANTOINE [27, 28] and NATHAN [27, 29]. The optimal choice of the basis depends mainly on states and properties we want to calculate. For our knowledge, we can mention some other codes: GLASGOW [30], VEC SSE [31], MSHELL [32], REDSTICK [33], RITSSCHIL [34], OXBASH [35] and DUPSM [36].

II.2. sd shell nuclei

sd shell nuclei have a number of neutrons N and protons Z between 8 and 20 (magic numbers). The sd nuclei region is located between the two doubly-magic nuclei ^{16}O and ^{40}Ca , this area contains 146 experimentally known nuclei 20 among them are stable [19]. At low excitation energies, the experimental spectra of these nuclei are characterized by the coexistence of normal positive parity states as well as the intruder negative parity states.

The nucleus to be study in this thesis is ^{28}Si , situated in the middle of the silicon isotopic chain area and it is a stable nucleus with $N=Z$. Figure II-7 presents the chart of sd shell nuclei where ^{28}Si is marked in red.

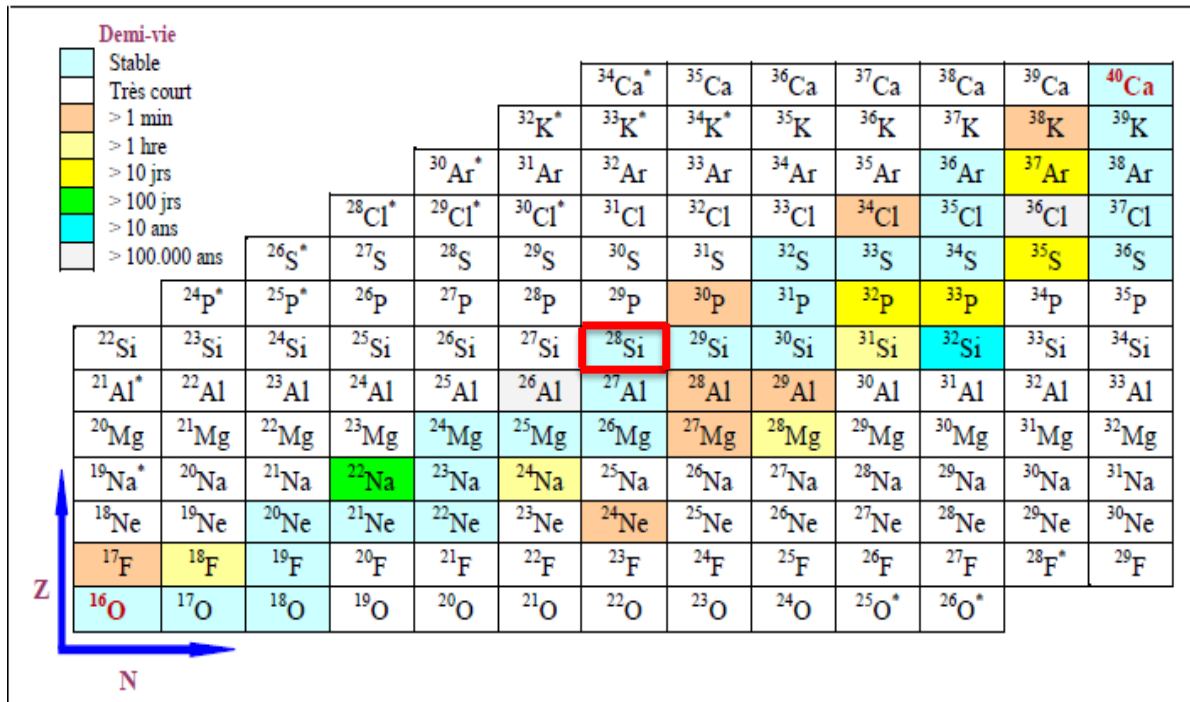


Figure II-7: Chart of sd shell nuclei [19].

At low excitation energy, the experimental spectra of these nuclei are characterized by the coexistence of normal positive parity states as well as the intruder negative parity states.

II.2.1. sd-shell nuclei states

II.2.1.1. Normal states

The shell model reproduces many aspects of nuclear structure for nuclei with mass range between 17 and 39; this model treats the valence nucleons within the two orbitals s and d, the p subshells are filled with the nucleons of the inert core, ^{16}O . These 16 nucleons of oxygen stay inactive, which implies the configuration 0 particle-0 hole (0p-0h). The corresponding states have positive parity and are so-called normal states or $0\hbar\omega$ states [19].

II.2.1.2. Intruder states

➤ Positive parity intruder states

In an sd nuclei, we can find positive parity intruder states which the configuration is out of the sd valence space and possess a configuration (2p-2h) for the $2\hbar\omega$ states or (4p-4h) for the $4\hbar\omega$ states, the corresponding nucleus is generally deformed. These effects observed in the doubly magic nuclei, ^{16}O , and ^{40}Ca .

➤ Negative parity intruder states

The intruder states with negative parity results from the promotion of one nucleon from p to sd or from sd to pf, these states are also called 1p-1h or $1\hbar\omega$ states. The interaction describing the $(0+1)\hbar\omega$ states is the PSDPF interaction [19, 37]. In this case, the model space

is full p-ds-pf space and the inert core is ^4He . These states appears at low excitation energies [19]. Figure II-8 shows a chart of sd nuclei with known negative parity intruder states.

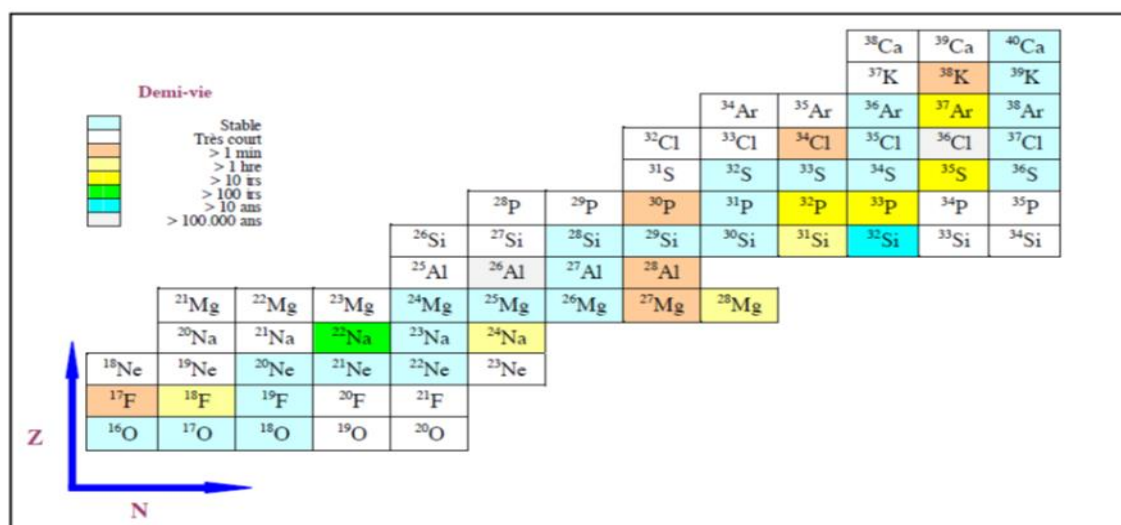


Figure II-8: sd nuclei with known negative parity intruder states [19].

II.3. PSDPF interaction

The shell model using USDA/B interactions [38] succeeded in the description of normal positive parity states of sd nuclei within sd model space with ^{16}O inert core.

Concerning the negative parity intruder states, the PSDPF interaction, developed by M. BOUHELAL [19, 37], in which the model space is composed of 3 major shells p, sd and pf with a ^4He core, describes consistently both the $0\hbar\omega$ and $1\hbar\omega$ states [37].

II.3.1. Shell model ingredients in case of sd-shell nuclei

- ❖ Valence space: the full p-sd-pf space.
- ❖ Compatible interaction with this space: PSDPF interaction.
- ❖ Code of calculation: the shell model code NATHAN [27, 29].

II.3.2. Positive and negative parity states description

The interaction describing consistently the normal + and intruder – parity states across the entire sd shell is the PSDPF interaction developed. In this description, the used core is restricted to the nucleus ^4He and the valence space includes the p, sd and pf shells containing the following nine sub-shells: $1p_{3/2}$, $1p_{1/2}$, $1d_{5/2}$, $2s_{1/2}$, $1d_{3/2}$, $1f_{7/2}$, $2p_{3/2}$, $1f_{5/2}$ and $2p_{1/2}$ [19, 37].

The sd shell nucleus that interested us in our thesis is the ^{28}Si . In this nucleus, the ground state 0^+ corresponds to the fulfilling $1d_{5/2}$ sub-shell, i.e. containing 12 nucleons (6 protons

and 6 neutrons). Figure II-9 presents an example of the first excited positive- and negative-parity states, 2^+ and 3^- , respectively, in ^{28}Si .

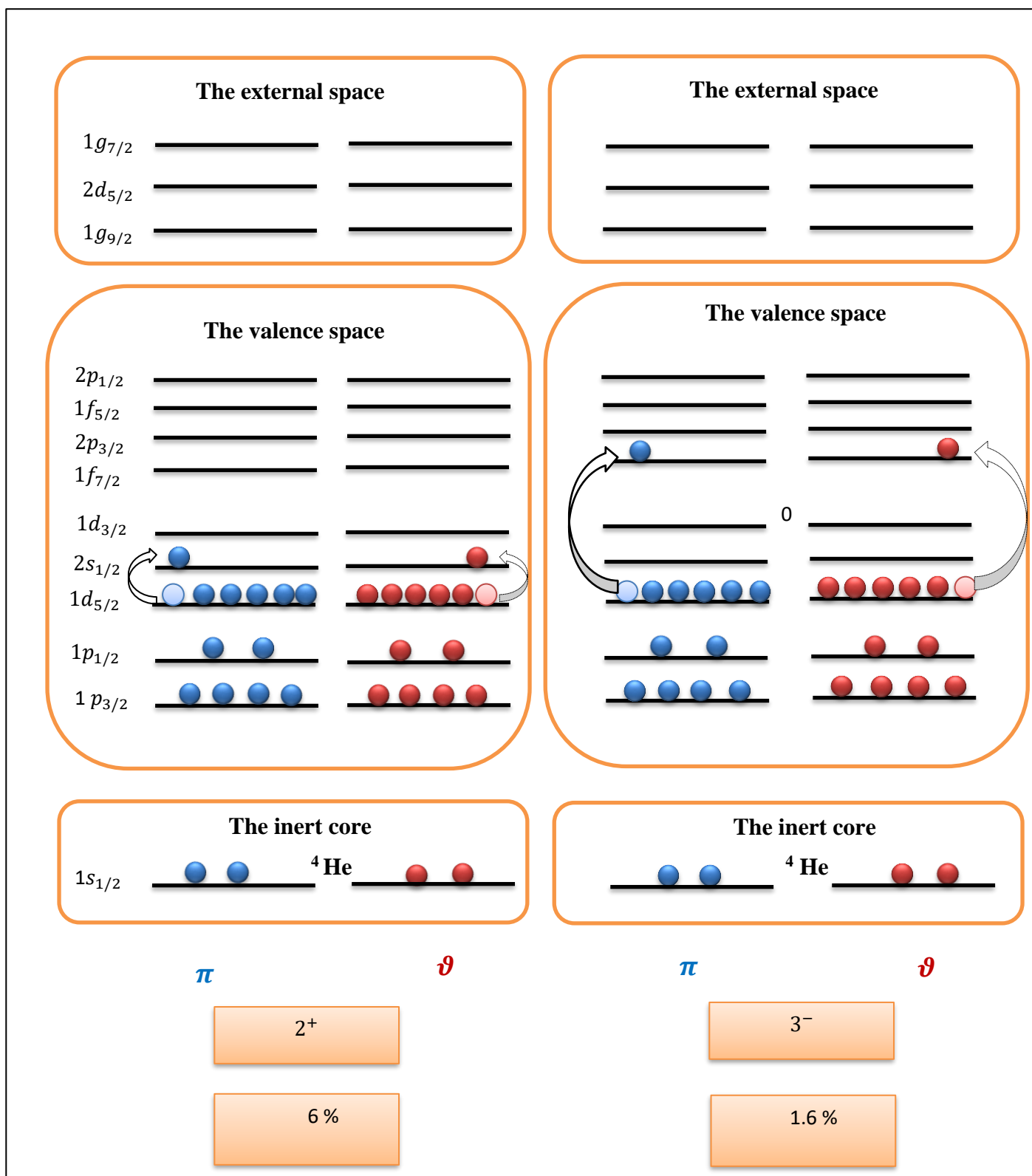


Figure II-9: Configurations of the first excited states 2^+ and 3^- in $^{28}_{14}\text{Si}$.

- ✚ The first positive excited state 2^+ , results from the jump of a proton or a neutron from the $1d_{5/2}$ sub-shell towards the $2s_{1/2}$ sub-shell with a probability of 6%.
- ✚ The first negative excited state 3^- , results from the promotion of a proton or a neutron from $1d_{5/2}$ to $1f_{7/2}$ with a probability of 1.6%.

Note that these two states have fragmented wave functions corresponding to small probabilities because this nucleus has $N=Z$ and, in the other hand, it has a lot of valence nucleons which enlarge the number of nucleon distributions within sd sub-shells.

II.3.3. Isospin

Neutron and proton has almost the same mass ($M_n/M_p=1.0014$), the same spin $S=1/2$ and the same nuclear properties. In 1932, Heisenberg proposed that proton and neutron could be considered as two different charge states of the same particle, the nucleon. Heisenberg assumed two values of isospin variable in order to distinguish between them, $t_z = 1/2$ for neutron and $t_z = -1/2$ for proton, where t_z denotes the projection of the isospin $t=1/2$ on OZ axis [25]. The electric charge of a nucleus is given by the following equation:

$$Q = \sum_t^Z q_p = Ze \Rightarrow Z = \frac{Q}{e} \Rightarrow T_z = \frac{A}{2} - Z = \frac{A}{2} - \frac{Q}{e} \Rightarrow Q = \left(\frac{A}{2} - T_z\right) e \quad (17)$$

Where Q denotes the electric charge of a nucleus, T_z the projection of the nucleus' isospin T on OZ axis and A is the number of nucleons. While T_z is given by the following value:

$$T_z = \frac{1}{2}(N - Z) \quad (18)$$

II.4. Electromagnetic transitions

The electromagnetic transition (E.M.T) properties may in, principle, be described by the nuclear model, and provides, accordingly, interesting information on calculated wave function of states between which the transition is made.

A nuclei formed in nuclear reaction is generally found in different excited states. If these states are related, their de-excitation towards the ground states, most of the time, done by the emission of gamma rays " γ " [19].

In this section, we will present the selection rules, operators and probabilities of the electromagnetic transitions.

II.4.1. Selection rules

In electromagnetic transition of a nucleus between the initial level (excitation energy E_i , angular momentum J_i , parity π_i) and the final level (excitation energy E_f , angular momentum J_f , parity π_f); gamma photon " γ " is emitted by a nucleon with energy E_γ , angular momentum L and parity π_γ [25]:

$$E_\gamma = E_i - E_f \quad (20)$$

$$|J_f - J_i| \leq L \leq J_f + J_i \quad (21)$$

$$\pi_i \pi_\gamma \pi_f = +1 \quad (22)$$

The figure II-10 presents the previous rule obviously:

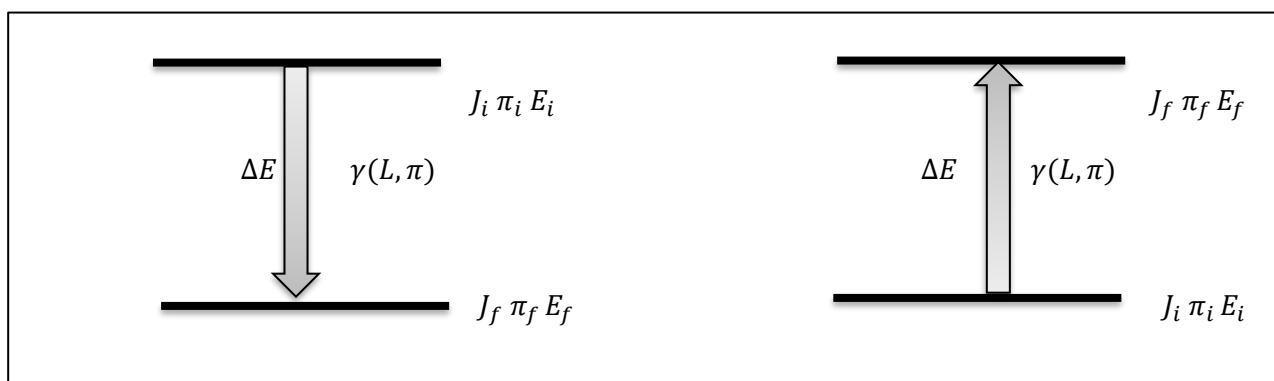


Figure II-10: Gamma emission and absorption of a nucleus.

We note that transition " γ " between $J_i = J_f = 0$ is forbidden by selection rules, which mean that L is different of 0.

The angular momentum of a transition L is also called multipolarity of radiation. The radiation character 2^L is dipolar for $L = 1$; quadrupolar for $L = 2$, octupolar for $L = 3$ etc...

The multipole is of electric type EL when $\pi_\gamma = (-1)^L$ and magnetic type ML when $\pi_\gamma = (-1)^{L+1}$. Therefore, " γ " transition that connects states of the same parities will get EL pairs and ML impairs, those connecting states of different parities have even EL and odd ML . The different transitions are listed on Table II-2 [25]:

L	π_γ	Radiation type	Label
1	-1	Electric dipole	E1
1	+1	Magnetic dipole	M1
2	-1	Magnetic quadrupole	M2
2	+1	Electric quadrupole	E2
3	-1	Electric octupole	E3
3	+1	Magnetic octupole	M3

Table II-2: Gamma transition multipolarity.

II.4.2. Operators

II.4.2.1. Electric operator

$$O_{LM} = \sum_{i=1}^A e(k) r^L(k) Y_{LM}(r(k)) \quad (23)$$

$e(j)$ is the free electric charge of a neutron j ; $e(j)$ equals “0” for “neutrons” and “e” for “protons” [25].

II.4.2.2. Magnetic operator

$$O_{LM} = \sum_{i=1}^A \mu_N \left[g^S(k) \vec{s}(k) + \frac{2g^l(k)}{L+1} \vec{l}(k) \right] \cdot \nabla(k) r^L(k) Y_{LM}(r(k)) \quad (24)$$

μ_N is the nuclear magneton, with $\mu_N = \frac{e\hbar}{2mc}$

$g^l(k)$ and $g^s(k)$ denote the orbital and spin gyromagnetic factors

The free orbital g factors have the following values [25]:

✓ For a proton:

$$*g^s(k) = 5.586$$

$$*g^l(k) = 1$$

✓ For a neutron:

$$g^s(k) = -3.826$$

$$g^l(k) = 0$$

II.4.3. Electromagnetic transitions probabilities

The reduced transition probabilities expressions are given by [25]:

$$B(EL) = \frac{9}{4\pi(L+3)^2} e^2 R^{2L} \frac{\Gamma_\gamma}{\Gamma_w} \quad (e^2 fm^{2L}) \quad (25)$$

$$B(ML) = \frac{90}{\pi(L+3)^2} \mu_N R^{2L-2} \frac{\Gamma_\gamma}{\Gamma_w} \quad (\mu_N^2 fm^{2L-2})$$

Where: $R=1.2A^{\frac{1}{3}} (fm)$, e : the electric charge, Γ_γ : Transition width and Γ_w : Weisskopf estimates (in eV).

Table II-3 presents the Weisskopf single-particle widths Γ_w (in $W.u.$) [25].

Electric	Magnetic
$\Gamma_W(E1) = 68A^{2/3}E_\gamma^3$	$\Gamma_W(M1) = 21E_\gamma^3$
$\Gamma_W(E2) = 4.9 \times 10^{-5}A^{4/3}E_\gamma^5$	$\Gamma_W(M2) = 1.5 \times 10^{-5}A^{2/3}E_\gamma^5$
$\Gamma_W(E3) = 2.3 \times 10^{-11}A^2E_\gamma^7$	$\Gamma_W(M3) = 6.8 \times 10^{-12}A^{4/3}E_\gamma^7$
$\Gamma_W(E4) = 6.8 \times 10^{-18}A^{8/3}E_\gamma^9$	$\Gamma_W(M4) = 2.1 \times 10^{-18}A^2E_\gamma^9$
$\Gamma_W(E5) = 1.6 \times 10^{-24}A^{10/3}E_\gamma^{11}$	$\Gamma_W(M5) = 4.9 \times 10^{-25}A^{8/3}E_\gamma^{11}$

Table II-3: Weisskopf single-particle widths Γ_W (W. u.) in MeV [25].

Notes:

- If the initial state decreases to different final states, then the total transition width Γ_T is the sum of the partial widths: $\Gamma_T = \sum_k \Gamma_{\gamma k}$ (25)
- The reduced probability of a transition B(E2) allows to figure out if the transition is due to an individual or collective contribution of nucleons in the nucleus. Indeed, the B(E2) is rather weak for a spherical nucleus and higher for a collective or deformed nucleus.
- The half-life according to the average-life is given by:

$$T_{1/2} = \tau_m \cdot \ln 2 \quad (26)$$

II.4.4. Electromagnetic transitions in sd nuclei

PSDPF interaction succeeded in the description of the $(0+1)\hbar\omega$ states in sd shell nuclei. Electromagnetic transitions are useful for the test of the wave functions. As it was mentioned previously, the E.M.T operators need the parameters: effective charge and gyromagnetic factors. Transitions between positive parity states E2 and M1 have been studied using USDA/B interactions [38]. Transitions connecting opposite parity states can be studied using the $(0+1)\hbar\omega$ PSDPF interaction.

In the first step, M. LABIDI has studied the E3 transitions by adjusting its effective charges to available experimental values [39]. The obtained parameters for the three transitions are presented on the Table II4.

W. A. Richter and B. A. Brown[38]		M. Labidi [39]
Effective charges (E2)	Gyromagnetic factors (M1)	Effective charges (E3)
$e_p = 1.36$	$g_{lp} = 1.159$	$e_p = 1.36$
	$g_{sp} = 5.150$	
$e_n = 0.45$	$g_{ln} = -0.090$	$e_n = 0.48$
	$g_{sn} = -3.550$	

Table II-4: Adjusted parameters for the transitions E2, M1 and E3.

In this chapter, we presented the basic notions of the shell model; the interactions developed to reproduce the spectroscopic properties and structure of the sd-shell nuclei. The last part of this chapter was dedicated to the electromagnetic transitions.

In the last chapter, we are going to calculate the spectroscopic properties of ^{28}Si using the PSDPF interaction.



Chapter III

Chapter III

Shell model description of ^{28}Si energy spectrum

In the previous chapter, we exposed a short review about nuclear models and the shell nuclei characteristic. In this chapter, we are interested to the description of the spectroscopic properties of ^{28}Si in the shell model framework.

We calculated the energy spectrum of ^{28}Si up to excitation energies of astrophysical interest then compared it to the experimental one. The electromagnetic transitions of the first + states in this nucleus were also calculated. Our purpose is the precisely examination of the experimental spectrum in order to determinate the ambiguous states. The results of our study will be presented and discussed after a short experimental review of ^{28}Si available data.

III.1. Experimental review of ^{28}Si energy spectrum

The adopted levels of ^{28}Si were published in 2013 Refs. [40, 41]. The ^{28}Si energy spectrum is well known up to 9.5 MeV excitation energy. Since this nucleus has an astrophysical interest, so we decided to calculate its spectrum up to 13 MeV because states from 10 to 13 MeV are crucial to calculate the astrophysical reaction rates. This spectrum contains a total of 128 states. In the energetic interval of astrophysical interest, there are 99 states. Among them, 93 uncertain (with non-confirmed parity) states, 4 certain (with known parity) states, and 2 unknown parity states.

In this data sheet, the author has collected all the information found in previous articles with some updated information. As an example, in 1995 a probability of $J^\pi = 4^+$ was found for the energy level observed at 10.945 MeV [42], which is still unconfirmed in 2013 data sheet [40]. Hence, the probability of $J^\pi = 6^+$ was found for the observed energy level at 12.860 MeV in 1995 [42], but it is changed in 2013 to $J^\pi = (2^+, 3^+)$ probabilities.

Since that, the main goal of researches in nuclear physics is to confirm the non-determined states. In 2015, J^π assignments were confirmed and other were proposed for the states related to the energy levels having an astrophysical interest. The old and new J^π assignments are shown on Table III-1 [43].

After that, almost of all the J^π assignments were confirmed, which are listed on Table III-2 [44].

Energy levels [MeV]	Old parity states	New confirmed parity states
8.259	$2^{(+)}, 6^{(+)}$	2_5^+
9.165	(4^+)	4_3^+
10.946	(4^+)	4_7^+
11.331	(6^+)	6_3^+
11.510	(6^+)	6_4^+
12.865	$(2^+, 3^+)$	6_6^+

Table III-1: J^π assignment states in 2015 [43].

Energy levels [MeV]	Old parity states	New parity states
10.182	(3^-)	3^-
10.190	$(5^-, 3^-)$	5^-
10.210	(3^+)	3^+
10.272	(0^+)	0^+
10.311	(4^+)	4^+
10.376	$(3^+, 4^+)$	3^+
10.418	(5^+)	5^+
10.515	(2^+)	2^+
10.541	(3^-)	3^-
10.596	(1^+)	1^+
10.668	$(2^+, 3^+)$	$3^+, (2^+)$
10.669	4^+	4^+
10.725	(1^+)	1^+
10.778	$1^+ \text{ to } 5^+$	$1^+ \text{ to } 5^+$
10.806	(2^+)	0^+
10.884	$(2, 3^+)$	$(2, 3)$
10.900	(1^+)	1^+
10.916	(3^-)	3^-
10.945	(4^+)	4^+
10.953	$1 \text{ to } 4$	2^+
10.994(3)	$(1, 2^+)$	1^-
11.078	(3^-)	0^-
11.101	(6^+)	6^+
11.142	(2^+)	0^+
11.196	(4^+)	4^+
11.242(6)		

11.266	(3 ⁻)	3 ⁻
11.296	(1 ⁻)	1 ⁻
11.333	(6 ⁺)	6 ⁺
11.388		
11.515	(2 ⁺)	2 ⁺
11.584	(3 ⁻)	3 ⁻
11.657	(2 ⁺)	2 ⁺
11.669	(1 ⁻)	1 ⁻
11.778	(2 ⁺)	2 ⁺
11.899	(2 ⁺ , 3 ⁻ , 4 ⁺)	4 ⁺
11.981	1 To 3	(2 ⁺ , 3 ⁻ , 4 ⁺)

Table III-2: Updated J^π assignments obtained in 2020 [44].

Notes:

When talking about astrophysics, we should mention the two following main reactions that occurs in massive stars and produces ^{28}Si .

✓ $^{24}\text{Mg}(\alpha, \gamma)^{28}\text{Si}$ reaction or the α -process: this reaction plays a role in stellar environments, namely in X-rays bursts, during carbon burning, at temperature varying from 0.5 to 2 GK. In massive stars ^{24}Mg is produced during carbon burning via the $^{20}\text{Ne}(\alpha, \gamma)^{24}\text{Mg}$ reaction following the conversion of two ^{12}C nuclei into ^{20}Ne by the reaction chain $^{12}\text{C}(^{12}\text{C}, p)^{23}\text{Na}(p, \alpha)^{20}\text{Ne}$. ^{24}Mg is subsequently destroyed by neutron or α -particle capture to make ^{25}Mg and ^{28}Si , respectively. It is necessary to update the astrophysical reaction rate for $^{24}\text{Mg}(\alpha, \gamma)^{28}\text{Si}$ incorporating recent modifications to the nuclear level data for ^{28}Si , and to determine if any additional as-yet unobserved resonances could contribute to the reaction rate. This latter, at temperatures relevant to carbon burning and Type I x-ray bursts, is well constrained by the available experimental data. This removes one reaction from the list of eight previously found to cause variations in x-ray burst light-curve calculations [44]. The energy range issued from this reaction for ^{28}Si comprises from 10.18 and 11.98 MeV.

✓ $^{27}\text{Al}(p, \gamma)^{28}\text{Si}$ reaction or the p-process: was originally thought to be proton-capture process; nuclei exposed to high temperatures and proton fluxes might capture protons to produce the p-nuclei. Researchers noted that disintegration would form the p-nuclei. If an initial distribution of r and s nuclei is exposed to a high temperature for a long time enough, all the nuclei melt, but, if the melting is quenched before it is complete, a distribution of proton rich nuclei results. Researchers found that the actual reaction sequence was a series of (γ, n) reaction followed by a (γ, p) and (γ, α) cascade down the proton rich side the β stability valley; this gamma process occurs in type II and I supernovae [45].

Figure III-1 presents a diagram for the p-process in ^{27}Al and the decay of ^{28}Si [46]. The capture reactions $^{25}\text{Mg} (p, \gamma)^{26}\text{Al}$, $^{26}\text{Al} (p, \gamma)^{27}\text{Al}$ and $^{27}\text{Al} (p, \gamma)^{28}\text{Si}$ are members of the hydrogen-burning MgAl cycle, which is of significant astrophysical interest. The energy spectra of this reaction starts experimentally at $E=4.979$ MeV by shooting ^{27}Al with a proton, and ends with a series of disintegrations to ^{28}Si in the ground state at $E=0.0$ MeV.

This chain of reactions can operate in stellar sites at much lower temperatures by various detailed models of massive main-sequence stars [47].

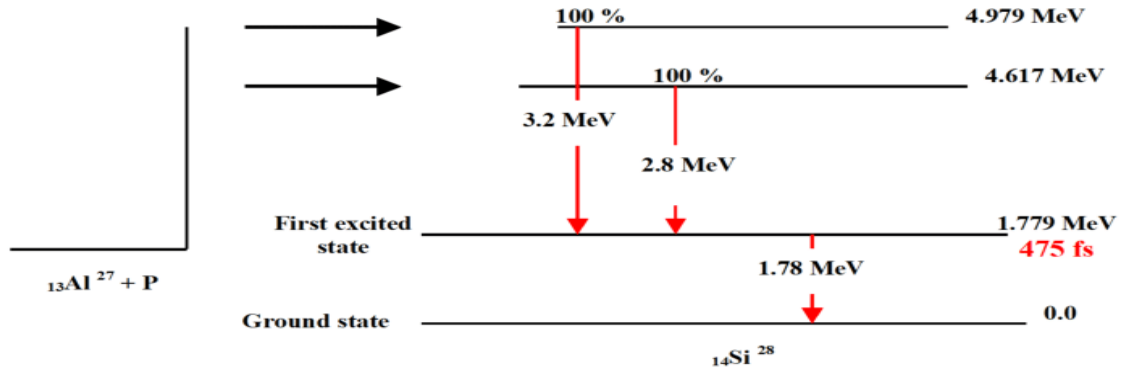


Figure III-1: Schematic diagram of the proton rich process in ^{27}Al and the decay of ^{28}Si [46].

III.2. Results and discussion

III.2.1. Energy spectrum

Investigation of nuclear properties and the laws governing the structure of nuclei is an active and productive area of physical research. In this work, we collected the experimental excitation energies; spins and parities J^π of ^{28}Si , with $N=Z$, up to 13 MeV. We remind that nuclei with even- A number of nucleons have a $J^\pi = 0^+$ ground state.

Aston discovered ^{28}Si in 1920 [48]. The experimental energy spectrum of ^{28}Si is presented in Table III-3, contains up to 13 MeV in total 128 levels. Among them 60 states have certain J^π , 66 states with uncertain J^π , and all the rest have undefined J^π . The J^π of states with (^o) and asterisk (^o) were confirmed in Refs. [43] and [44], respectively, those with (^o) were taken from Ref. [49].

We calculated, using the PSDPF interaction and the code NATHAN, the excitation energy spectrum and the electromagnetic transition properties of the first $0\hbar\omega$ states in ^{28}Si . The comparison of the obtained excitation energies to the experimental data [40, 41] is shown on Table III-3. Note that $\Delta E1 = E_{\text{th}}(\text{PSDPF}) - E_{\text{exp}}$. A comparison to the calculated excitation energies, using USDA and SDPFMW interactions, taken from Refs. [43] are also presented on Table III-3. Note that $\Delta E2 = E_{\text{th}}(\text{USDA}) - E_{\text{exp}}$ and $\Delta E3 = E_{\text{th}}(\text{SDPFMW}) - E_{\text{exp}}$.

Since ^{28}Si is a self-conjugate nucleus with $N=Z$, it has $T=0$ and 1 states. States with $T=1$ can be obtained by comparison of the excitation energies in the isobaric $A=28$ triplet ^{28}Al , ^{28}P

and ^{28}Si . Note that PSDPF is a coulomb free and isospin independent interaction so it gives the same results for all the T=1 in A=28 nuclei, ^{28}Al , ^{28}P and ^{28}Si . The ground states in the mirror nuclei ^{28}Al and ^{28}P are 3^+ states. The T=1 states are presented in the last column.

J_i^π	PSDPF	Eexp	$\Delta E1$	USDA ³	$\Delta E2$	SDPFMW ³	$\Delta E3$	T=1 States
0_1^+	0	0	0					
2_1^+	1,8918	1,779	0,1128	1,94	0,161	1,99	0,211	
4_1^+	4,64487	4,618	0,02687	4,549	-0,069	4,659	0,041	
0_2^+	4,80094	4,98	-0,17906	4,821	-0,159	5,013	0,033	
3_1^+	6,46975	6,276	0,19375	6,46	0,184	6,163	-0,113	T=1
4_2^+	7,15943	6,888	0,27143	7,069	0,181	7,032	0,144	
3_1^-	7,17588	6,879	0,29688					
1_1^-	7,22714	8,905	-1,67786					
0_3^+	7,398	6,691	0,707	7,478	0,787	7,235	0,544	
2_2^+	7,55811	7,381	0,17711	7,524	0,143	7,521	0,14	
2_3^+	8,00076	7,416	0,58476					
3_2^+	8,11283	7,799	0,31383					
2_1^-	8,21884	8,819	-0,60016					
1_1^+	8,25723	8,328	-0,07077					T=1
3_2^-	8,45718	9,765	-1,30782					T=1
6_1^+	8,48944	8,544	-0,05456	8,395	-0,149	8,457	-0,087	
2_4^+	8,50591	7,933	0,57291					T=1
4_1^-	8,60341	8,413	0,19041					
2_5^+ ^3	8,67103	8,259	0,41203	8,86	0,601	8,665	0,406	T=1
5_1^-	8,7664	9,702	-0,9356					
3_3^+	9,2428	8,589	0,6538					
5_1^+	9,39057	8,945	0,44557	9,302	0,357	9,227	0,282	T=1
3_4^+	9,53477	9,316	0,21877					T=1

0_4^+	9,59008	8,953	0,63708					
4_3^+ 3	9,59994	9,165	0,43494	9,369	0,204	9,489	0,324	T=1
2_6^+	9,62367	9,382	0,24167					
2_7^+ 2	9,68469	9,479	0,20569					T=1
1_2^-	9,68779	9,929	-0,24121					
0_1^-	9,79529							
1_2^+	9,8906	9,496	0,3946					T=1
4_4^+	9,98999	9,417	0,57299					
5_2^- 1	10,0864	10,19	-0,10359					T=1
5_2^+ 1	10,3199	10,418	-0,09809					
2_2^-	10,3809	10,668	-0,28712					
3_5^+ 1	10,6018	10,209	0,39282					T=1
0_5^+	10,6204	10,272	0,34839					
2_8^+ 3	10,6441	9,796	0,8481	10,693	0,897	10,688	0,892	
2_3^-	10,6884	10,883	-0,19457					T=1
4_2^-	10,7026	11,243	-0,54044					
1_3^+ 1	10,7096	10,596	0,11358					
6_1^-	10,7376	11,576	-0,83842					
0_6^+ 1	10,7736	10,806	-0,03239					
1_3^- 1	10,7828	10,944	-0,16117					
3_6^+ 1	10,7937	10,376	0,41771					
4_5^+ 1	10,8322	10,311	0,52117					
2_9^+ 1	10,9384	10,514	0,42436					T=1
1_4^+ 1	10,9604	10,725	0,23537					
1_5^+ 1	11,0443	10,9	0,14426					T=1
5_3^-	11,0716	11,934	-0,86242					
3_7^+ 1	11,0745	10,668	0,40652					

2_4^-	11,0953	11,388	-0,2927					
3_3^- 1	11,1775	10,182	0,99549					
$6_2^+ 1$	11,1963	11,1	0,09626					
4_6^+	11,2266	10,668	0,55864					T=1
3_4^- 1	11,2928	10,541	0,75175					
2_{10}^+ 1	11,3845	10,953	0,43151					
1_4^- 1	11,4708	11,296	0,17476					
2_5^-	11,4926	11,8	-0,30745					
2_{11}^+	11,5466	11,433	0,11355					
1_6^+	11,5782	11,446	0,13223					
$6_3^+ 3$	11,6211	11,332	0,28914	11,531	0,199	11,508	0,176	T=1
4_7^+ 3	11,6267	10,944	0,68266	11,841	0,897	11,55	0,606	T=1
4_8^+ 1	11,6485	11,195	0,45352					
4_3^-	11,7723	11,435	0,33726					
1_7^+	11,8387	12,331	-0,49231					
3_5^- 1	11,8809	10,916	0,96485					T=1
3_8^+	11,9286	10,778	1,15055					
$0_7^+ 1$	11,9807	11,142	0,83866					
2_{12}^+ 1	11,994	11,516	0,47797					
4_9^+	12,0364	11,572	0,46438					
6_2^-	12,0366							
6_4^+ 3	12,056	11,51	0,54602	11,953	0,443	11,815	0,305	
5_3^+	12,1441	11,779	0,3651					
5_4^+	12,2122	12,175	0,03718					
4_{10}^+	12,2148	11,781	0,43383					
0_2^-	12,2209							
2_6^-	12,2427	12,073	0,16968					

3_9^+	12,2774	12,24	0,03737					
3_6^- 1	12,3074	11,079	1,22838					
1_5^- 1	12,3525	11,67	0,68251					
2_{13}^+ 1	12,3652	11,657	0,7082					
3_{10}^+	12,3882	12,295	0,09321					
4_{11}^+	12,4464	11,867	0,57936					
0_3^-	12,482							
1_8^+	12,5425	12,715	-0,17249					
4_4^-	12,5881	12,204	0,38408					
5_4^-	12,5888	12,023	0,56575					
1_9^+	12,6162	12,755	-0,13883					
6_5^+	12,6452	12,152	0,49318					
5_5^+	12,6962	12,817	-0,12085					
4_{12}^+	12,8123	11,9	0,91233					
3_{11}^+	12,8495	12,542	0,30751					
7_1^-	12,9111							
2_{14}^+ 1	12,9298	11,779	1,15078					
7_1^+	12,9411	13,117	-0,17592					
5_5^-	12,9721	12,643	0,32913					
3_{12}^+	12,9993	12,636	0,36333					
0_4^-	13,0076							
1_6^-	13,0615	12,182	0,87948					
4_5^-	13,0654	12,664	0,4014					
0_8^+	13,113	12,266	0,84696					
3_7^- 1	13,2272	11,265	1,96221					
2_7^-	13,2495	12,216	1,03351					
3_{13}^+	13,2904	12,867	0,42342					
2_{15}^+	13,3021	11,986	1,31605					
1_7^-	13,4066	12,805	0,6016					
6_6^+ 3	13,4776	12,859	0,61861	13,423	0,564	13,591	0,732	

4_6^-	13.4901	12.99	0.50012				
4_{13}^+	13.4987	11.976	1.52268				
2_{16}^+	13.8169	12.016	1.80087				
4_{14}^+	13.8437	12.241	1.60267				
3_{14}^+	13.9682	12.917	1.05123				
3_8^- 1	13.9743	11.585	2.38913				
0_9^+	13.9837	12.976	1.00768				
2_8^-	14.072	12.318	1.75395				
6_7^+	14.2663	12.994	1.27227				
4_{15}^+	14.3031	12.325	1.97812				
2_{17}^+	14.354	12.071	2.203				
3_{15}^+	14.4028	12.924	1.47879				
1_8^-	14.5354	12.815	1.72044				
4_{16}^+	14.6868	12.475	2.21179				
2_{18}^+	14.9186	12.29	2.62862				
3_9^-	14.9449	12.195	2.74985				
1_9^-	15.229	12.974	2.25495				
2_{19}^+	15.3305	12.301	3.02946				
4_{17}^+	15.3454	12.551	2.79438				
4_{18}^+	15.8226	12.855	2.96762				
3_{10}^-	15.8535	12.489	3.36449				
2_{20}^+	16.0313	12.441	3.59025				
4_{19}^+	16.4664	12.9	3.5664				
2_{21}^+	16.7084	12.574	4.13443				
3_{11}^-	17.3156	12.743	4.57262				
2_{22}^+	17.4125	12.726	4.68652				
2_{23}^+	18.1045	12.902	5.00252				
3_{12}^-	18.5646	12.803	5.76155				
2_{24}^+	18.8533	12.924	5.92933				

Table III-3: The energy spectrum of the ^{28}Si .

On Table III-4, we present the calculated high spin states and compared to available data.

J_i^π	PSDPF	Eexp	$\Delta E1$	USDA ³	$\Delta E2$	SDPFMW ³	$\Delta E3$
8_1^+	14.16	14.463	-0.4833	14,305	-0.338	14.212	0.431
7_2^+	14,354	13,71	0,6439	14,352	0.642	14.374	0.664
9_1^+	18.401						
8_1^-	15.113						
9_1^-	17.077						

Table III-4: High spin states

The PSDPF interaction had a great success in describing the 0 and 1 $\hbar\omega$ states of the studied nucleus. Some discrepancies between calculation and experiment have been found and are interpreted as follows:

- States with $\Delta E > 400$ keV, in red, have a collective contribution (more than 0p-0h configuration). This situation is expected starting from the fourth state of each J^π .
- States with $\Delta E > -400$ keV, in bleu, are not well reproduced using PSDPD.
- Two degenerated states having $J_i^\pi = 3_1^+$ and 2_2^- have been observed at 10.668 keV.
- The 0^- states are not observed in ^{28}Si .

III.2.2. Electromagnetic transitions

Using the PSDPF interaction, we calculated the electromagnetic transition properties of the first excited positive parity states in ^{28}Si nucleus. The comparison between the obtained results and experimental data [41] are presented on Table III-4. All the calculated mean lifetimes have the same order of magnitude as experimental ones. We can also see the good agreement between states concerning the branching ratio.

J_i^π E(exp) (MeV)	J_f^π (Exp) _f (MeV)	T1/2 (Exp)	T1/2 (SM)	Mult (Exp)	R (Exp) (%)	Mult (SM)	R (SM) (%)
1.779 2_1^+	0.0 0_1^+	4.75E-13	3.70E-13	E2	100	E2	100
4.618 4_1^+	1.779 2_1^+	3.7E-14	2.48E-14	E2	100	E2	100
4.98 0_2^+	1.779 2_1^+	3.50E-14	2.59E-14	E2	100	E2	100
6.276 3_1^+	1.779 2_1^+	7.80E-13	2.14E-12	M1+E2	88.2	M1+E2	77.3
	4.618 4_1^+			M1+E2	11.8	M1+E2	22.7

Table III-5: Comparison experimental [41] versus calculated spectroscopic properties of the ^{28}Si .

Conclusion:

We have used the PSDPF interaction to study the spectroscopic properties of the ^{28}Si .

From this study, we can conclude the following points:

- The comparison of our results to the observed excitation energies shows a good agreement. PSDPF interaction allowed us to very satisfactory reproduce the normal and intruder states.
- This study enabled us to predict the J^π assignments for ^{28}Si and to have an idea about the degenerated states and collective contribution.

This study gives more credit to the PSDPF interaction in reproducing the spectroscopic properties of nuclei even in the middle of the sd shell which could not been included in its fit.



Conclusion

Conclusion

Nuclear physics is an important pursuit because the study of the atomic nucleus is at the heart of our ability to understand the universe. It provides answers and expands our knowledge of both the infinitely small and the extremely large. We are interested in our work, to ^{28}Si nucleus situated in the middle of the silicon isotopic chain, which is also situated in the middle of sd shell nuclei zone.

The main aim of our work was the calculation of the energy spectrum of ^{28}Si up to 13 MeV. The electromagnetic properties of the first states were also calculated and compared to available data.

The comparison experiment versus theory of the excitation energies shows, in general, a quite well agreement of the obtained results. This study allowed us to confirm some uncertain states and to predict J^π assignments for the unknown states.

In conclusion, we can say that the PSPDF interaction successfully described the spectroscopic properties of this nucleus.



Bibliography

Bibliography

- [1] Opportunities in nuclear astrophysics”, Conclusions of a Town Meeting held at the University of Notre Dame, 7-8 June 1999. Prepared by the Joint Institute for Nuclear Astrophysics Michigan State University and the University of Notre Dame.
- [2] Doroth et al, Formation and Evolution of the Universe,| AMNH, Part of Hall of the Universe, “Educator's Guide to the Cullman Hall of the Universe, Heilbrunn Cosmic Pathway, and Scales of the Universe”.
- [3] <https://energyeducation.ca/encyclopedia/Silicon>
- [4] R. Casten et al., Nuclear Structure and Astrophysics Town Meeting Draft 2.0 Oakland, CA November 9-12, 2000.
- [5] A. Z. Jones., thoughtco.com/stellar-nucleosynthesis-2699311.
- [6] K. S. Krane. Oregon State University. Introductory nuclear physics.
- [7] S. E. Woosley, W. D. Arnett, D. D. Clayton. "The Explosive burning of oxygen and silicon". The Astrophysical Journal Supplement Series. (1973)
- [8] D. D. Clayton, Principles of Stellar Evolution and Nucleosynthesis. University of Chicago Press. pp. 519– 524. (1983)
- [9] S. Woosley and T. Janka, Nat. Phys, 1, 147 (2005).
- [10] Safety Data Sheet for Silicon Enriched Silicon, According to ISO 11014:2010.
- [11] Clarivan Larivan Science. Silicon, atomic structure - Stock Image - C018/3695.
- [12] P. Picozza et al, PAMELA – A payload for antimatter matter exploration and light-nuclei astrophysics, Astroparticle Physics.27 (2007) 296–315.
- [13] S. Gundacker, A. Heering, “The silicon photomultiplier: fundamentals and applications of a modern solid-state photon detector “, Phys. Med. Biol. **65** (2020) 17TR01.
- [14] <https://www.rsc.org/periodic-table/element/14/silicon>.
- [15] A. Das and T. Ferbel, Introduction To Nuclear And Particle Physics , World Scientific (2003).
- [16] B. Povh, K. Rith, C. Scholz and F. Zetsche, Particles and Nuclei: An Introduction to the Physical Concepts, Springer, 6th edition (2008).
- [17] M. G Mayer, phys. Rev. 75, 1969 (1949).
- [18] O. Haxel, J. H. D. Jensen and H. E. Suess, phys. Rv.75, 1766 (1949).
- [19] M. Bouhelal, Ph.D. Thesis, under joint supervision of University of Batna, Algeria, and University of Strasbourg, France (2010).
- [20] K. J. R. Rosman and P. D. P. Taylor, Pure and App. Chem. 70, 217 (1998).
- [21] <http://hyperphysics.phy-astr.gsu.edu/hbase/Nuclear/shell2.html#c1>

- [22] K. Heyde, “The nuclear shell model”; study edition. Second Corrected and Enlarged Edition
- [23] N. D. Cook, “Models of the Atomic Nucleus”; department of informatics; Kanasai University; Takatsuki.
- [24] K. S. Mc. Elvain, Ph.D. Thesis, under the supervision of University of California, Berkeley (2017). “Harmonic Oscillator based effective theory, connecting LQCD”
- [25] P.J. Brussaard, P.W.M. Glaudemans, “Shell–Model Applications in Nuclear Spectroscopy”, North–Holland (1977).
- [26] A. Goasduff, Ph.D. Thesis, University of Strasbourg, France (2012).
- [27] E. Caurier, G. Martinez–Pinedo, F. Nowacki, A. Poves, A. P. Zuker, *Rev. of Mod. Phys.* 77, 427 (2005)
- [28] E. Caurier, F. Nowacki, *Acta Phys. Pol. B* 30, 705 (1999).
- [29] E. Caurier, G. Martinez–Pinedo, F. Nowacki, A. Poves, J. Retamosa, A. P. Zuker, *Phys. Rev. C* 59, 2033 (1999).
- [30] R. R. Whitehead, A. Watt, B. J. Cole, I. Morrison, *Adv. Nucl. Phys.* 9, 123 (1977).
- [31] A. Schmidt et al., *Phys. Rev. C* 62, 044319 (2000).
- [32] T. Mizusaki, RIKEN Accelerator Progress Report Vol. 33, 15 (2000).
- [33] E. W. Ormand, C. W. Johnson, REDSTICK code, 2002.
- [34] D. Zwarts, *Comp. Phys, Comm.* 38, 365 (1985).
- [35] B. A. Brown et al., MSU–NSCL Report No. 524 (1985).
- [36] A. Novoselsky, M. Vallières, Drexel University Shell–Model Code DUPSM (1997).
- [37] M. Bouhelal, F. Haas, E. Caurier, F. Nowacki, and A. Bouldjedri, *Nucl. Phys. A* 864, 113 (2011).
- [38] B. A. Brown, W. A. Richter, *Phys. Rev., C* 74, 034315 (2006).
- [39] M. Labidi, Master’s Thesis, University of Tebessa, Algeria (2013).
- [40] M. S. Basunia, *Nucl Data sheets*, 114, 1189 (2013). Adopted levels, Gammas for ^{28}Si .
- [41] <http://www.nndc.bnl.gov/nudat2>
- [42] J. Brenneisen et al., *Z Phys. A* 352, 403-415 (1995).
- [43] S. S. Bhattacharjee et al., *Phys. Rev C* 91, 044306 (2015)
- [44] P. Adsley, A. M. Laird and Z. Meisel, *Phys. Rev. C* 102, 015801 (2020)
- [45] Bradley S. Meyer, Jason S. Brown, Nigo Luo, ASP conference series, vol. 99, 1996.
- [46] <https://www.researchgate.net/figure/Aschematic-diagram-for-the-proton-capture-process-in-Al-27-and-the-decay-of-Si-28>
- [47] Ch. Iliadis et al., *Nucl. Phys A* 512 (1990) 509-530 North-Holland
- [48] F. W. Aston, *Nature* 105, 547 (1920).
- [49] S. Adachi et al., *Phys. Rev C* 97, 014601 (2018).